BENEMERITA UNIVERSIDAD AUTONOMA DE PUEBLA
FACULTAD DE CIENCIAS FISICO-MATEMATICAS

Search for Monotop Production in Events with One Lepton, Missing Transverse Energy, and Jets

Tesis presentada al

Colegio de Física

Como requisito parcial para la obtención del grado de

Licenciado en Física

Por

Diana Leon Silverio

Directora de Tesis

Dra. Maria Isabel Pedraza Morales

Puebla, Pue.
Noviembre 2018

BENEMERITA UNIVERSIDAD AUTONOMA DE PUEBLA
FACULTAD DE CIENCIAS FISICO-MATEMATICAS

Search for Monotop Production in Events with One Lepton, Missing Transverse Energy, and Jets

By

Diana Leon Silverio

A thesis submitted to

Colegio de Física

in fulfillment of the requirements for degree of

Licenciado en Física

Supervised by

Ph.D Maria Isabel Pedraza Morales

Puebla, Pue.
Noviembre 2018

Acknowledgements

This thesis is dedicated to all people who supported me and provide me their affection, during their development. I would like to start by thanking my parents. They are and will be the most important part of my life. Thanks for letting me follow my dreams and take my own desitions. I know that sometimes see their little baby grow up is hard but both have to believe in me. You should be certain that raised me with strong roots.

To my brothers, Saul and Jorge. I consider myself extremely lucky for have you. Both are the best part of my life. Thanks a lot for be with me every step of my way, for your support and motivation. Thank you for caring for me, resist my temper tantrums, comfort me, but above all else thanks for make me happy. Believe me that I cannot imagine my life without my gorditos.

To my advisor, Isabel Pedraza. I would like to express my gratitude for your supporting my academic career. I would like to thank that you accepted me as your student without knowing me. That changed my life and set me in the place that I currently am. I can tell you that it was one of the most important decisions of my life. In a nutshell, thanks for believe in me.

I wholeheartedly to my colleagues who were with me at Fermilab, thanks for become to part of my life. Matteo and Bo, thanks for giving me the opportunity to return to Fermilab and provide me a full experience. Sudha thanks for considering me as you close friend, I was lucky to meet you. I promise you that I will give my best to be able to find you again. Tim thanks for caring me last months. I know that it is not your style but thanks for staying with me when I needed. Finally, this is for you Sonaina, thanks for your continuous support and motivation. If you are reading this, trust me!! this would not have been possible without you. You have a special place in my heart and you will always have it. I am grateful that you let me in into your family environment and let me met your little son. I can not imagine what my life would have been without you two. Thanks for caring my soul and make happy.

To my friends at University, Thanks for share experiences with me. My student life has been fun thanks for you. Part of my personality is due to your affection and appreciation that you show me all the time. I do not have enough words to say how grateful I am. Especially, Mario, you have been with me in the worst and best moments of my life. I can affirm that you know me very well (that includes my dramatic personality) and in spite of that, you are by my side at every step. Thanks for letting me be part of your life. For providing to my heart consolation when I am lost. You allowed me to find new ways and I will always grateful with you. Furthermore, you introduce me Oscar, thanks because now I consider him as my close friend. I was really lucky to found both guys. Finally, Thanks to Julio, Marquito, Cinty, Will, David, Ruheri, Mariana, Silvia, Oscar pequeño, Oscar grande and Manuel, for sharing your experiences with me. Julio you are the best, never doubt it!!. Marquito you are bobito, sorry it is the truth. Cinty, simply love you.

In closing, to Jan. Thanks for coming to Mexico and helped me finish this thesis. To be honest, for a moment I thought this was not going to finish until you arrived, Thanks!!.

Abstract

In this research, we study the possibility of detecting new physics phenomena at the Large Hadron Collider (LHC) looking for a leptonic monotop production through flavor changing neutral current channel, in order to confirm a possible Dark Matter particle. Particularly, we focus in events with final states of one lepton, missing transverse energy and at least one single jet tagged as originating form a b-quark. This study consider pp collisions at 13 TeV in centre-of-mass energy with a total integrated luminosity of 35.9 1/fb, which was recorded in 2016. The analysis presented here has been carried out using the CMS official software framework for event generation, simulation, and reconstruction. The search strategy is formulated based on the characteristics of the main kinematics variables. As result, the exclusion limit shows that this kind of signal with a luminosity of 35.9 1/fb can be excluded in a range between 1000 and 2500 GeV, with a cross section bigger than 6 pb.

Keywords: LHC, Monotop, Dark Matter, CMS

Contents

1. Introduction

The Standard Model (SM) of particles physics is a theory that explains almost all elementary particles and their interactions. It has been able to predict new particles that experimentally have been confirmed; nevertheless, there are many questions left unanswered that are waiting to be solved. In the recent years, the particle physics studies turned its attention to signatures aimed at unusual fi states which are difficult to measure or have not been considered yet [31].

In this work, we consider events with a specific example of a V-field in order to study the fla vor violation for a possible solution of the Dark Matter (DM) problem of the SM [38]. Searches for monotop associated with of DM production have been constrained for Fermilab Tevatron data by the CDF [15] collaboration as well as the CMS [30] and ATLAS [12]. In the present study, we focus on events where a single top quark is produced in association with a large amount of missing energy, where the top quark that decays into a bottom quark and a W boson, and W boson decays into one lepton with its neutrino. This kind of process is special because the productions with this fi state is cleaner, turning into a suitable candidate for search new physics.

In order to revisit and improve previous analysis of the LHC sensitivity to monotop, this analysis has been restricted to consider solely monotop decaying into a purely leptonically final state with an integrated luminosity of 35.9 fb^{-1} of data due to proton-proton collisions at the center-of-mass of 13 TeV, collected by the CMS experiment in 2016.

2. Literature review

From the early 1950s, Quantum Electrodynamics (QED) had become a reliable theory. However, many years passed before Quantum Field Theory (QFT) could be applied to physical problems of interest. This serious change gave rise to describe electromagnetic force, the weak and strong interactions. The lagrangians were *reinvented* adding new classes of particles or quantum fields. New concepts had to be introduced, mainly connected by non-Abelian gauge theories and spontaneous symmetry breaking. At present, the strong, weak and electromagnetic interactions of elementary particles had been established by Standard Model (SM), which have a similar structure as QED. For example, the SM, this theory is associated with the Gauge group $SU_c(3) \times SU_l(2) \times U_Y(1)$ and is consider the theory of elementary particles. This chapter presents an overview of the SM, we will highlight their principal properties. Subsequently we will tackle one on the most important bullets, Physics Beyond the SM (BSM) in order to introduce the dark matter signatures.

2.1. The Standard Model

The SM of the particle physics is a theory that describes three of the four fundamental interactions in the Universe. Established in 1970s the SM implements special relativity and quantum mechanics based on quantum field theory. The local symmetries are strictly correlated with strong, weak, and electromagnetic interactions, which are described by Abelian and non-Abelian gauge theories. The SM is currently main theory which has been tested at stunning levels; such as the discovery of top quark in 1995 [13] and Higgs boson in 2012 [28], in this manner the SM is establishing as the best fundamental understanding of the phenomenology of the particle physics.

2.1.1. Main ingredients of SM

The SM involve seventeen fundamental particles, these are characterized by their quantum numbers, spin and mass. In the SM framework the visible matter is coming from two kinds of elementary particles, quark and leptons. They are fermions (spin-1/2) and obey the Pauli exclusion principle which establish that two or more fermions cannot occupy the same place at the same time. We must also emphasize that each fermion has an antiparticle with the same mass but opposite charge, this means that fermions are distinguished by their charges under strong and electromagnetic interactions. As show the picture **2-1** the SM consider

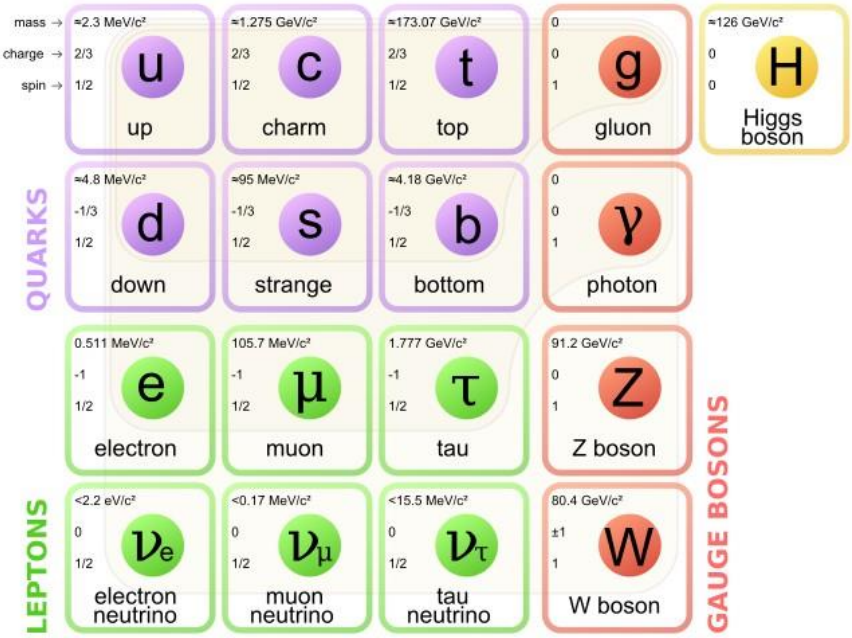

Figure 2-1.: Particle contents of Standard Model

6 leptons and 6 quarks, their interactions are mediated by integer spin particles called gauge bosons. The main feature of quarks is that they carry color charge in addition to electromagnetic charge and weak isospin, allowing them interact with others particles via strong force. It is establish that quarks cannot exist individually rather, inside that they are able to form composite particles called mesons (quark doublets) and baryons (quark triplets) which in general are called hadrons. Information of quarks listed in the table **2-1**.

Quarks	Discovered	Electric Charge
up (u)	1968	+2/3
down (d)	1968	-1/3
charm (c)	1970	+2/3
strange (s)	1968	-1/3
top (t)	1995	+2/3
bottom (b)	1977	-1/3

Table 2-1.: SM quarks and their properties

The last six fermions are called leptons and do not carry color charge. An important subgroup of leptons are neutrinos, they are massless and come in three fla vors, and correspond to their partner leptons, i.e. electron, muon and tau neutrino. They are at least six order of magnitude lower on their mass than all of the other SM fermions and their interaction are not allowed under the strong and the electromagnetic force because they are neutrals, as a result their detection is challenging. Relevant information of the leptons is present in the table **2-2**.

The interactions are mediated by four gauge boson (spin-1), generally know as force me-

Lepton	Discovered	Electric Charge	Mean life
electron (e)	1897	-1	STABLE
electron neutrino (ν_e)	1956	0	
muon μ	1936	-1	$2.197E^{-6}$
electron neutrino (ν_μ)	1962	0	
tau (τ)	1975	-1	$291\pm1.5E^{-15}$
tau neutrino (ν_τ)	2000	0	

Table 2-2.: SM leptons and their properties

diator particles. They do not obey the Pauli exclusion principle, and as result they do not have any theoretical restriction on their spacial density, explicitly the mediator are photon (γ), $W^{\pm}$, Z and gluons (Table **2-3**). The photon and gluon are massless, while the Z and W bosons are massive. Specifically, the electromagnetic interactions are mediated by photons, gluons mediates the strong interaction, while the weak interactions by $W^{\pm}$ and Z. Because the gauge bosons $W^{\pm}$ and Z have mass ($\approx$ 80 GeV and 90 GeV, respectively) weak interactions are weak at low energy. Despite their weakness, they give rise to differentiate signatures through their symmetries of the electromagnetic and strong interactions. It is important to mention that the gluon mediator carry color charge (red, green and blue). They comes in eight types and participate in the strong interaction.

Boson	Interaction field	Color Charge
photon (γ)	Electromagnetic	0
gluon (u)	Strong	8 colors
$W^{\pm}$	Weak	0
Z^0	Weak	0
Higgs (H)		0

Table 2-3.: SM bosons and their interactions

At high energies the electromagnetic and weak force are unified in the electroweak interaction. In 1962 and 1963 research studies indicated the electroweak symmetry would be broken in presence of an unknown field. The break mechanism is responsible that the fermions and the massive gauge boson acquire a specific mass. This phenomenology postulated the existence of a specific field (spin-0), which is consequence of a scalar massive particle called Higgs boson, theoretically proposed by Peter Higgs and Francois Englert in 1964 [36] and experimentally confirmed in 2012 [11]. Specifically the photon and gluon are not influenced by Higgs field because they are massless, though the Higgs boson can interact with its own field this is the reason that H^0 is massive.

2.1.2. Physics Beyond Standard Model

The SM had been successful, but is restricted to lower-energy. However, it leaves some phenomena unexplained, such as neutrino masses, baryon asymmetry, the hierarchy problem, CP-violation, and the nature of something that we call dark matter. The constant search of prima facie evidence to help answer these and others questions had been received special

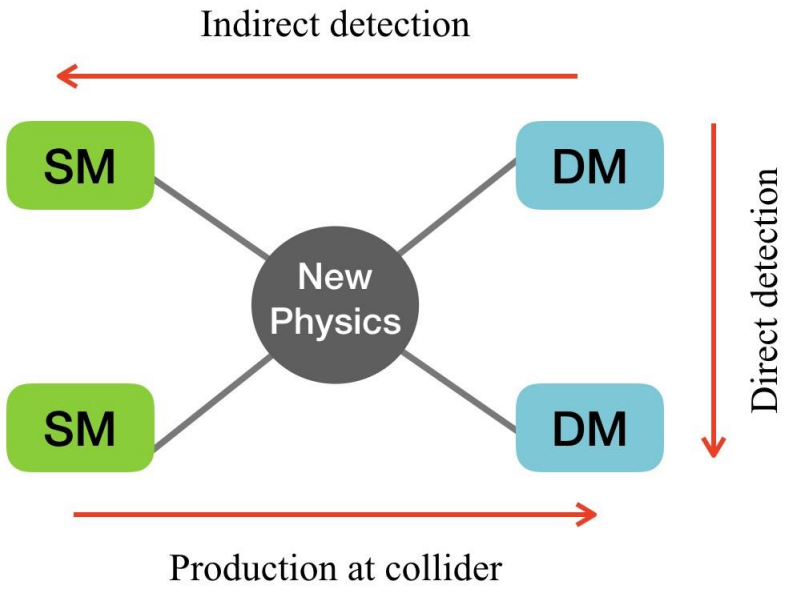

Figure 2-2.: Artistic view of three dark matter detection strategies

attention in the particle physics groups. Several theories had been established in order to detect physics beyond SM observations as derivations from SM predictions.

2.2. Dark Matter

Dark Matter (DM) is one of the most compelling pieces of evidence for physics beyond the SM. Cosmological observations demonstrate that around 85 % of the mass of the Universe is comprised of DM. These observations along with further constraints make it highly likely that DM is primarily composed of weakly interacting massive particles (WIMPs). If non-gravitational interactions exist between DM and SM particles, DM could be produced by colliding SM particles at high energy. In many theories, the pair production of DM particles in hadron collisions proceeds through a spin-0 or spin-1 bosonic mediator, with the DM particles leaving the detector without a measurable signature. One way to observe them is when they are produced in association with a visible SM particles.

Understanding the interaction between dark matter and SM particles occurs only through three principal techniques, as show in Figure **2-2**. The technique is strictly correlated with the couplings of interactions. This section aims to describe briefly these techniques.

2.2.1. Direct Detection

Direct Detection consider as the main technique. Its principle of operation is based on the idea that a galaxy is packed with WIMPs, these galactic WIMPs will pass through Earth and interact with special matter in the lab, while depositing energy to a single nucleus. The signal is measured through velocity and density of galactic WIMPs in the solar neighborhood as well as the cross section of WIMPs-nucleon scattering. The implementation of several detection techniques (observation of photon, scintillation and ionization) are necessary in order to measure the recoil of nucleus from dark matter scattering. Experiments CREST and CUORICINO are focused in observation of photon, while DAMA [44], ZEPLIN-I LIBRA and NAIAD correspond to scintillation techniques, lastly for ionization the main experiments are HDMS, GENIUS, MAJORANA, DRIFT and IGEX.

2.2.2. Indirect Detection

Direct detection of DM is not possible through accelerator such as LHC or the search of nuclear recoils due to dark-matter particles scatterings, but they can provide information of DM existence indirectly. The fi aim of indirect detection is to observe the radiation produced in dark matter self-annihilation, which plays an important role in the significant flux of γ-rays, neutrinos and antimatter [41]. In general, the radiation flux is directly proportional to the dark matter annihilations and dark matter density. It is possible search large radiation fluxes in regions where density of DM is significant.

DM annihilation can be the result of SM particles, but products which are charged particles are difficult to locate their radiation sources when they are under the effect of a magnetic field. However, their weak interactions allow the neutrinos search DM concentrations at center of massive astronomic objects, such as center of the Earth, the Sun or a galaxy. On other hand, γ-rays could be observed from center of Sun or Earth.

2.2.3. Production at Collider

The direct detection of DM in collider experiments is forbidden but its production at weak scale provides the possibility to detect it at the LHC. Collider searches linked to DM production are characterized by ”mono-objets”, for instance mono-jet, mono-photon or mono-top, which are accompanied by huge missing transverse energy. The characterization of DM searches established by Effective Field Theory (EFT), implements simplified models. The main thrust of these models is interpret the missing-energy signatures at collider and capture the relevant kinematics properties with only few parameters [8]. Particularly, the amount of energy produced in the collision give rise to almost all interactions are governed by electroweak and QCD multi-jet processes. This fact is applied in event selections and background processes. For example, the top-quark production, single top, QCD multi-jet and Diboson processes are negligible by kinematics cuts. Nevertheless, dominant backgrounds can’t be

removed and thus require a data driven techniques or Monte Carlo.

All previous techniques of DM detection have strengths and weaknesses. For instance, the direct and indirect detection signals lose most of their force in relation of DM candidate lighter due to remains energy.

3. Theoretical Framework

In the framework of the SM, the monotop kinematic distributions depend on the partonic initial state and the nature of the undetected objects. In general, the top quark is mainly produced at the Large Hadron Collider (LHC) due to loop-suppression and the Glashow-Illiopoulos-Maiani mechanism [5]. Viewed from the theoretical framework consider a top quark in the fi al state gives the possibility to fi the flavor of the fin al state and limit the possible partons in the final state, while experimentally the top quark signature provides an easier route to discriminate the no visible traces in the detector [38].

As a result, the production of monotop states can occur by means of two differ e n t mechanisms. This process is generally characterized by the nature of fi state particles in association with missing energy. In the fi scenario, the top quark is produced in association with an invisible fermion χ through the resonant exchange of colored scalar S, while the second exchange occurs via fla vor-changing vector fi V, as represented in Feynman diagram of Figure **3-1**.

Examples of the first class is consider an R-parity violating supersymmetry where the intermediate particle is a top quark decaying into a top plus a lightest neutralino or in SU(5) theories where a vector leptoquark V decays into a top quark and a neutrino. The second class provides the possibility to explain possible solutions of dark matter problem via fla vor-violating couplings of a bosonic mediator.

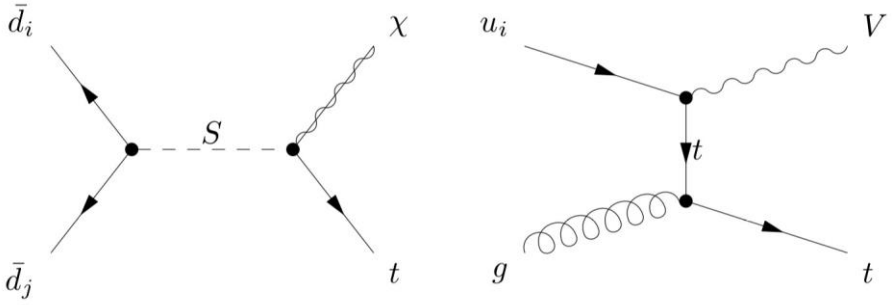

Figure 3-1.: Representative Feynman diagrams of monotop signatures, through resonant exchange of a colored scalar fi S (left) and via fla vor-changing neutral current V (right)

The present study focuses on the fla vor-changing neutral current (FCNC) model, where the main signatures associated with monotop production are associated with leptonically decaying top quark. This channel has branching fraction of around 32 %. Starting from the SM, in a simplified model approach, the monotop production mechanism could be described FCNC production by:

$$L_{int} = V_\mu \bar{\chi}\gamma^\mu(g^V_\chi + g^A_\chi\gamma^5)\chi + \bar{q}_u\gamma^\mu(g^V_u + g^A_u\gamma^5)q_u V_\mu + \bar{q}_d\gamma^\mu(g^V_d + g^A_d\gamma^5)q_d V_\mu + h.c. \quad (3\text{-}1)$$

where $h.c$ refers to the Hermitian conjugate of the preceding terms in the Lagrangian. We depict the heavy mediator as V and χ is the DM particle, which we assume is a Dirac Fermion. On the other hand, the q_u and q_d in terms of interaction quark-V, represent three generations of up-type (q_u) and down-type (q_d) quarks. The couplings g^V_χ and g^A_χ represent the vector and axial vector-coupling between χ and V, respectively. The interactions among V, u, c, and top quarks is modeled via two 3 × 3 flavor matrices vector- and axial vector-coupling, $g^u{}_V$ and g^u_A respectively, these matrices play an important role because the monotop production becomes possible owing to their off-diagonal elements. In order to preserve $SU(2)_L$ symmetry, the down-type couplings g^d_V and g^d_A must be analogous and satisfied:

$$g^u_V - g^u_A = g^d_V - g^d_A \quad (3\text{-}2)$$

Considering the above constraint 3-2, for convenience we assume $g^u_V = g^d_V = g^q_V$ and $g^u_A = g^d_A = g^q_A$. In order to yield the production of monotop state is required the only nonzero elements of g^u_V and g^u_A are assumed to be those between the fi and third generation.

It must be highlighted that in the current study consider a mediator V with spin 1 by exploring the undetectable vector boson associated with a single top signal and dark matter candidates. The statement of mediator V compels us to establish two possible scenarios, where the mediator could be lighter of heavier in contrast to the top quark. In the fi scenario consider a heavy mediator V in comparison with top quark, guarantee that mediator is not long lived as it can decay into a top quark. This makes possible include a decay channel into an undetectable state to be liable to note as dark matter candidate, whilst in the second case when V is lighter, there to be a kinematically forbidden in all possible decays modes into a top and lighter quark. In the minimal case, at tree-level, the mediator could decay into a multibody final states i.e $V \to u\bar{b}W^-$ or $V \to \bar{u}bW^+$, furthermore when m_V is lighter than m_W the W boson is virtual [37].

3.1. Signal Features

The main signatures of monotop production, is the top decay, described by

$$pp \rightarrow t + V \rightarrow bW + E_T^{miss} \tag{3-3}$$

where V is the spin-1 boson, (see Fig **3-1**) and E_T^{miss} denotes the missing transverse energy.

In this study we focus on leptonic top decay mode instead of the hadronic case, for two main reasons. Firstly, the leptonic backgrounds are cleaner, then they can be controlled and simulated reliably. Secondly, the hadronic mode has been large explored, in order to search new physicist is reasonable try to explore deeper the leptonic channel. For instance, we can suppress the QCD multijet background, which is difficult to model.
The main contribution in the final state comes from the top quark, the topology of signal is built for one b-jet, a lepton, a neutrino related to the lepton and the unobserved decay of the V.

$$pp \rightarrow t + V \rightarrow lb + E_T^{miss} \tag{3-4}$$

The CMS and CDF had made direct measurements of $t \rightarrow bW$ branching fraction of 100% [39, 3].

Consider a lepton in the fi state give rise to consider two signal regions. The fi case involve an electron as final state, while the second look at muon. This feature will be relevant at analysis level.

3.2. Principal backgrounds

The SM backgrounds are selected in relation to the physical objects of interest. The backgrounds present similar topology in their final state as the signal. Considering the previous statement, we listed the backgrounds, which are taking account in this analysis (Table **3-1**).

Consider events that involve a single top quark leading consider a significant amount of missing transverse energy (E_T^{miss}) originating from an invisible new state, where E_T^{miss} correspond to the negative vector sum of the transverse momenta of all visible objects. Nevertheless, the main discriminator variables are the transverse mass (M_T) and E_T^{miss} of lepton. The M_T is quantity which is invariant under Lorentz boost along the z direction, its definition can be rewritten in terms of the momentum of the triggered lepton (p_T) and E_T^{miss} as:

$$M_T = \sqrt{2p_T(R)E_T^{miss}(1 - \cos\Delta\varphi(p_T(R), E_T^{miss}))} \tag{3-5}$$

Background	Dynamic Method	Physics objects
$t\bar{t}$	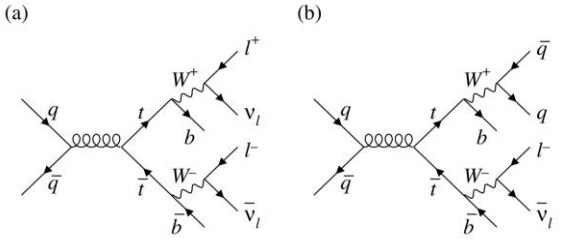	a) 2 leptons + 2 b-jets + E_T^{miss} b) 1 lepton + 1 b-jet + jets + E_T^{miss}
$W+jets$	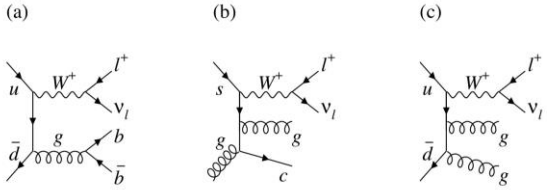	For a) b) and c) 1 lepton + jets + E_T^{miss}
$SingleTop$	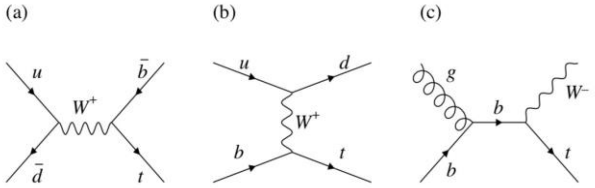	For a) b) and c) 1 lepton + jets + E_T^{miss}
$Z+jets$	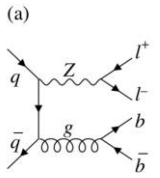	a) 2 leptons + jet + E_T^{miss}
$Diboson$	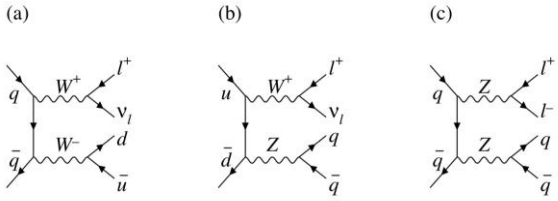	a) and b) 1 lepton + jets + E_T^{miss} c) 2 leptons + jets + E_T^{miss}
QCD	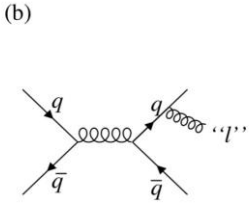	b) 1 fake lepton + jets + E_T^{miss}

Table 3-1.: Representative Feynman diagrams of backgrounds and their final physics objects

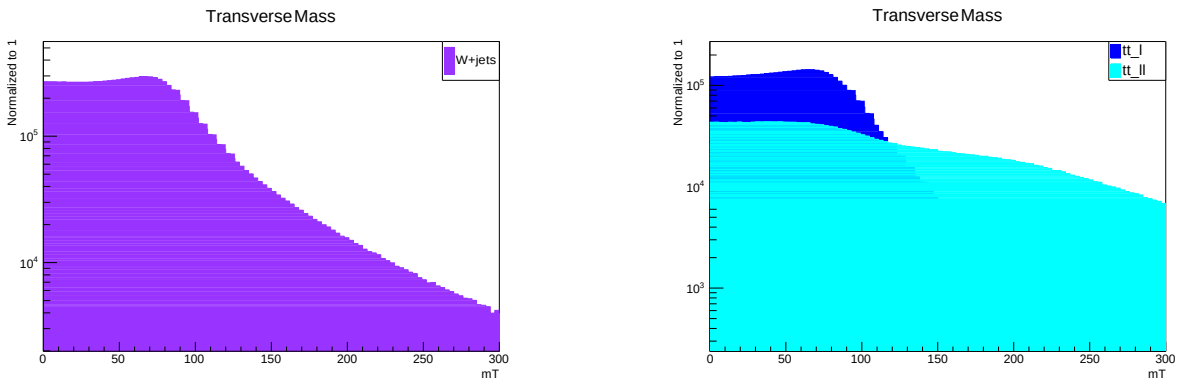

(a) (b)

Figure 3-2.: (a) Transverse mass of W+Jets background and (b) Transverse mass of $t\bar{t}$ background

where $\Delta\varphi$ denote the azimuthal angle between E_T^{miss} and $p_T(R)$. The end-point of the M_T spectrum is $M_T^{max} = M$[4], this particular feature is manifested in the main backgrounds (figure **3-2**), though the signal does not present this as a result of its two sources of missing energy, allowing the M_T becomes into a crucial point for distinguishing between signal and background.

3.2.1. Backgrounds Description

The main backgrounds are stricter correlated with the M_T. This sections is dedicated to show the importance of the M_T for each background. The specific situations of every backgrounds are listed bellow;

- **$t\bar{t}$** : The largest background comes from the SM production of $t\bar{t}$ pairs. Particularly, in the semi-leptonic decay mode the spectrum of M_T meets the characteristic of an end point $M_T^{max} = m_W$. On the other hand, in the dileptonic mode, if one of the leptons is missed, the one that is left can exceed a M_T of 80 GeV.

- **W + jets** : In this study we are looking for process with up to one jet in the fi state. These background are important, but can not become as the main background because their small acceptances after cuts. These process required a fake or real b-tagged jet, in order to contribute to the background. The nature of the jet depend of the working point of the b-tagging algorithm. Particularly, the b-mistag rate in current ATLAS and CMS is the order to 1/100 and 1/1000. This allows the background contribution be brought under control.

- **Z + jets** : This process is considering $Z \rightarrow (RR)$ as background when the leptons pass unseen and contribute to the signal like events.

- **Single top:** This is a subdominant background because it is irreducible, up to a jet that could come from ISR. Remembering that our main discriminator variable is M_T the sole top process which has a large M_T comes from of the production of tW ($pp \rightarrow tW \rightarrow bllv\nu$). If during the process a lepton is missed then M_T is a variable which is not constrained by m_W, in this way this process contribute to the background, however, due to has a low cross-section coverts it into the not largest background.

- **Diboson:** In particular this background is suppressed compared to the previous ones, because its cross-section is low. The process W^+W^- has the largest cross-section, and can only contribute if one W decays hadronically and the other one leptonically, this means that a b-jet can only originate from one of the W decays. In another case when we consider the WZ production is necessary to involve a leptonic W decay and a mistagged jet or a missing b jet from the $Z \rightarrow b\bar{b}$ decay in order to contribute. The last process is ZZ which has the smallest cross-section, in this case one Z should decay hadronically and the other one leptonically in order to fulfill the selection cuts; furthermore, the leptons should be missed and must also should be a mistagged jet or a missing b jet deriving from the Z hadronic mode. In general, generate events that consider values $M_T > m_W$ are not likely, for this reason this background is almost entirely negligible.

- **QCD:** The background deriving from QCD are consider suppressed since that the reconstructed leptons of these processes can only succeed throughout misidentified jets. Furthermore, consider a high p_T misreconstructed jets guarantees a large missing transverse energy. Considering the signal characteristics, a hight p_T jet veto has the faculty of suppresses the QCD missing energy turns out to very effective in neglecting this background to the leptonic monotop signature.

Misidentification of physics objects is an important source of backgrounds. It is important to measure this type of ”fakes”because is possible that this misidentification may not be accurately modeled in the MC.

In general, three main misidentification elements are mentioned below:

- **Fake jet:** The jet reconstruction algorithm uses energy deposits from ECAL and HCAL. However, some particles are reconstructed using the same information that the calorimeters provides. Then, sounds reasonable because misidentifications occurs. For instance, at high values of $\Delta\varphi$, muon and electron channel show a discrepancy identification. Because this is in the lepton-back-to-back regimen, this accounts for jet mis-measurements. Reconstruct fake jet candidates can come from hadronic tau decays, detector noise, pile-up contribution and cosmic ray.

- **Fake lepton:** These kind of fakes can present a high lepton p_T spectrum which makes part of the signal region. There are several different sources of lepton misidentification and depends on the lepton type. For example, the fake lepton can arise from charged hadrons, photon conversions, or semi-leptonic heavy-flavor decays.

- **Hadronization of b jet:** One main discrepancy is located in the muon channel. It is observed a low values of $\Delta\varphi$, where is possible obtain a muonic b-hadron decays. This muon is a real one, but is a muon that it is not relevant for our analysis.

The previous three misidentification are currently issues for all analysis. They are continuously studied and present a huge challenge for particle physics community. I could add a full chapter related to this topic and I still would not fully understand. However, this general view provide us an overview of how these situation can affects our analysis.

4. The CMS Experiment

The main purpose of the Compact Muon Solenoid (CMS) [16] experiment is to explore and understand particle physics at high energies, exploring proton-proton collisions produced at the Large Hadron Collider (LHC). CMS is one of the most import experiments of recent years and has been fundamental for search new physics. The detector is set up around a solenoid magnet and is characterized by its electromagnetic calorimeters and a quality tracking system. This chapter approach in a detailed way with the structure of the CMS detector, each sub-detector will be described individually allow to get a general idea of the structure and objectives of CMS experiment.

4.1. The Large Hadron Collider

The Large Hadron Collider (LHC) [18] is the most powerful collider and the largest in the world, it is built at the European Laboratory for Particle Physics (CERN) in Geneva, Switzerland. The LHC has two rings where particles are accelerated circularly through 26.7 km long tunnel which was built by Large Electron Positron Collider (LEP). Two counter-rotating provides a collision between proton-proton with $\sqrt{s}$ = 13 TeV that is the highest value recorded in the history of accelerator experiments. The protons are supplied in small bunches of approximately 10^{11} protons with spacing between them of 25 ns. The beams of proton can provide a collision at 4 diff t points (figure **4-1**), at each point a main detector is located.

- **ALICE** (A Large Ion Collider Experiment) Studies quark-gluon plasma that correspond to strongly interaction matter at extreme energy densities.
- **ATLAS** (A Toroidal LHC ApparatuS) The final general purpose experiment. It researches extra dimensions and possible candidates of dark matter particles.
- **CMS** (Compact Muon Solenoid) The second general purpose experiment. It studying the Standard Model, extra dimensions and possible dark matter particle candidates.
- **LHCb** (LHC-beauty) It is specialized in CP-Violation a thorough b quarks.

In addition to these four main experiments, there are others, in particular Centauro And STrange Object Research (CASTOR) and TOTal and Elastic Measurement (TOTEM) [32]. They share the experimental cavern with CMS and common trigger.

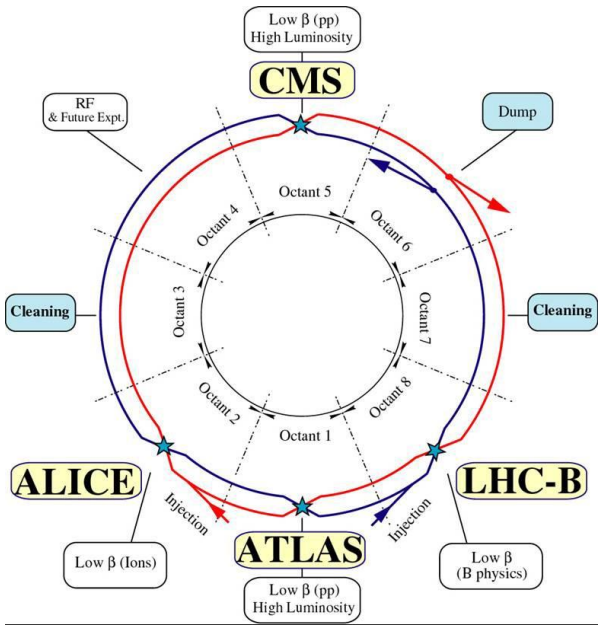

Figure 4-1.: Map of the LHC accelerator ring and detectors

4.2. The CMS Detector

The Compact Muon Solenoid is a multipurpose experiment at the LHC. It's designed cylindrically with a full length of 21.6m, a diameter of 15m with an inner diameter of 6m and a superconducting solenoid able to provide 4T magnetic fi reaches a total weight of 12 500 tonnes.

The CMS detector is made up of sub-detectors as show Figure **4-2**. The sub-detectors are set up around the interaction region forming concentric layers where each sub-detector contributes specific aspects for reconstruction of the collision event. The tracking system, electromagnetic calorimeter (ECAL) [17] and hadronic calorimeter (HCAL) [18], these are sub-detectors constitute the inner layer of the solenoid. The out layers are composed of diff t muons chambers and the endcap sections is located the calorimeters called forward hadronic calorimeter (HF).

The detector geometry use a right-handed coordinate cartesian system, with the center of the detector is the origin and x-axis pointing to the center of the LHC ring, the z-axis in direction of CMS cylinder axis and the y-axis is perpendicular to the plane of the ring. The cylindrical design of the detector and the invariant description of pp physics allows to use a pseudo-angular reference frame, given a polar angle θ, which define to the positive z-axis and φ the azimuthal coordinate relative to x-axis allowing to define the pseudorapidity defined as $\eta = -ln[tan(\theta \backslash 2)]$ [29].

According to the fi **4-2**, we can have a general idea of the design of the detector, the overall descriptions of sub-detectors will be reviewed in the following.

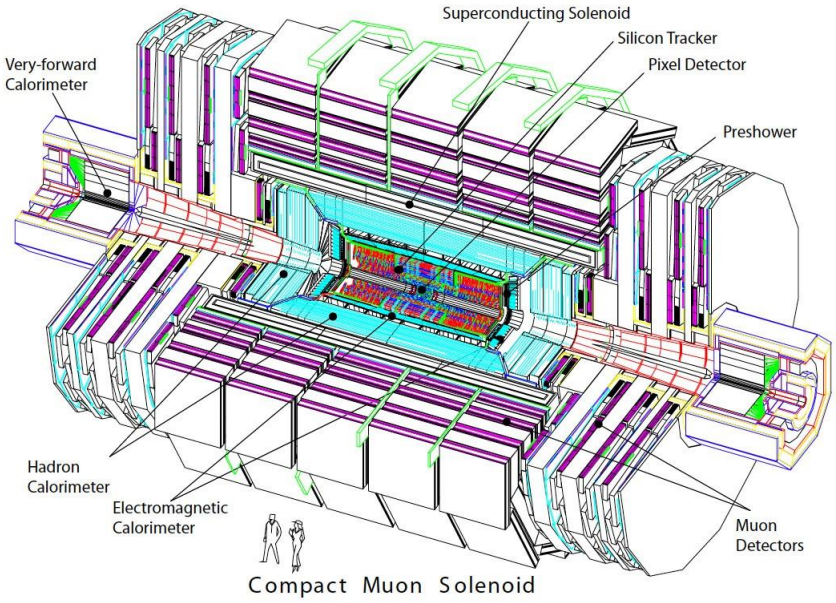

Figure 4-2.: Overview of the Compact Muon Solenoid

- **Tracker r < 1.1 m $|\eta| < 2.5$** Its volume is set by 5.8 m in length and 2.5 m in diameter, roughly 15 148 silicon modules built the strip tracker, which cover 198 m^2 total area of active silicon detectors. Its aims is reconstructing tracks created by charged particles [29].
- **ECAL 1.1 m < r < 1.8 m $|\eta| < 3$** The electromagnetic calorimeter is composed by $PbWO_4$ scintillating crystals, which provide a quality resolution of tracks measurements from electron and photons [17].
- **HCAL 1.8 m < r < 4 m $|\eta| < 5$** The hadron calorimeter system measures energy from jets. Located on both sides of the detector is placed the HF that covers a range $3 < |\eta| < 5$ [32].
- **Superconducting magnet r < 4 m** $|\eta| <$ **1.5** This produces a uniform magnetic fi of 4T, composed of wire coils. The tacker, ECAL, and HCAL are accommodated inside to the magnetic coil [19].
- **Muon System 4 m < r < 7.4 m $|\eta| < 2.4$** The aims of muon chambers are measure muons tracks, composed 250 drift tubes (DTs), 540 cathode strip chambers (CSCs) in the endcaps, and 610 resistive plate chambers (RPCs) [20].

4.2.1. Magnetic system

The CMS superconducting magnet [19] is roughly 10 800 tonnes (considering the coil), 13 m long with a diameter of 5.9 m and magnetic field of 4 Teslas. The yoke diameter is 14

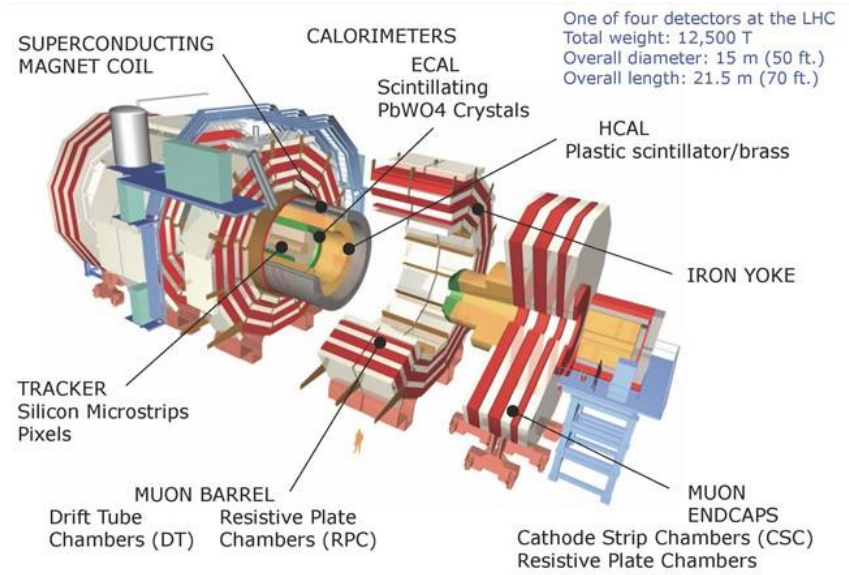

Figure 4-3.: Structure of CMS detector at LHC

m while axial yoke length is 21.6 m, nevertheless in the outermost disk of the endcap is produced 1.7 Teslas. The description of CMS magnet refers to magnet yoke, vacuum tank and superconducting coil.

- **Superconducting coil:** The superconducting coil system is defined as the coil and the ancillary subsystems required for its operation. The reinforced conductor of 4 layer CMS coil is capable of sustaining by itself all the induced magnetic forces.
- **Magnet Yoke:** The yoke has two components; barrel yoke and endcap, this corresponds the cylinder around the superconducting coil and the disk that closes the barrel respectively.
- **Vacuum tank** It is made of stainless steel thick cylinder of 60 mm, where reside two concentric cylindrical shells, the outer shell is situate in inner part of the central barrel ring.

4.2.2. Silicon tracker

The tracker [21] provides a quality resolution of tracks from charged particles and a good identification of primary and secondary interactions vertex. The CMS tracker covers a radio of 115 cm with a length of 270 cm start from interaction point to outside. The transverse momentum measurement of high isolated tracks in the barrel region ($|\eta|$ <1.6) has a resolution $\delta p_T/p_T \approx (15 \cdot p_T \oplus 0.5)\,\%$ and gradually decreases to $\delta p_T/p_T \approx (60 \cdot p_T \oplus 0.5)\,\%$ in the endcaps ($|\eta|$ <2.4).

The tracker system was developed for satisfying resolution in spite of the fast decrease of particle density hence two technologies are implemented, pixel vertex and silicon strip tracker.

Pixel Vertex

The pixel detector [21, 22] are instruments of choice for the tracking of charged particles close to the interaction point at the LHC. The pixel system considers at least two hits for exploring the tracker with sterling precision for that propose the pixel vertex was built of the two sections.

- *Pixel Inner Barrel (PIB)*: The PIB consist of three layers placed to radii of 4.1 - 4.5 mm, 7.0 - 7.4 cm and 10.7 - 11.2 cm and they make an approximately total 768 pixel modules. A single pixel is a square of area 150μm × 150μm. Its spacial resolution is around 10μm.

- *Pixel Inner Endcap (PED)*: The PED has two endcap disks on each side located at $|z|$ = 34.5 cm and contains a total 672 pixel modules. Its spacial resolution is 20μm.

Silicon strip tracker

The Silicon Strip Tracker (SST)[42, 22] is made up micro-strips devices footprint longitudinally for about 5.6 m length and 2.4 m in diameter, covering a $|\eta| \leq 2.5$. The silicon micro-strip covers approximately 70m^2 with 15 148 silicon modules, each silicon detectors has diff t sizes and pitches. The strip tracker includes four subsystems (Figure **4-4**):

- *Tracker Inner Barrel (TIB):* The TIB consist of four cylindrically layers. The strings of three thin modules are mounted within and out of the half-shells.

- *Tracker Inner Disk (TID)* The TID consist of three inner disk per side, with three rings of modules per disk. Those inner disk are located between TIB and TEC.

- *Tracker Outer Barrel (TOB)* The TOB is a rod. It is made of six layers, of which carried either three double-sided or three single-sided thick modules on each side.

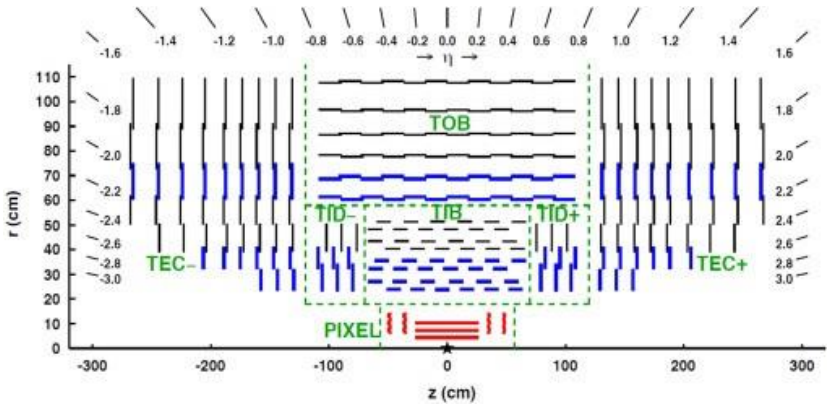

Figure 4-4.: Several detectors in the silicon tracker. Silicon pixel detector is shown in red, whereas silicon strips detector are denoted by TIB, TID, TOB and TEC are shown in blue and black

- *Tracker Endcaps (TEC)* The TEC is made of nine disk of carbon fib er (CF) fitted. The basic substructure of the TEC is petal. A wedge shaped CF support plate which carries up to 28 modules arranged in up to seven radial rings. The SST has two endcaps.

Due to high particle density, the silicon detectors can produced a radiation, which produce a significant damage in detector efficiency. For example, the pixel and strip detector components are affected for radiation emitted themselves. In order to counter the damage, the silicons detectors work at a temperature of -10°C, which allowing to establish a long term operation. Allowing register an efficiency around 88 % from jets with a fake track of 0.1 %. Moreover, the single tracks register 99 % of efficiency.

4.2.3. Electromagnetic calorimeter

The Electromagnetic Calorimeter (ECAL) [17] play a fundamental role for any general purpose LHC experiment, principally for electroweak symmetry breaking through of the Higgs sector.

The CMS electromagnetic calorimeter is hermetic scintillating crystal calorimeter composed by lead tungstate $PbWO_4$, which have a small radiation length (X_0 = 8.9 mm) and Molière radius of 21.9 mm. The scintillation decay time is approximatively 10 ns allowing to collect 80 % of total light which is produced after pp collision over a period of 25 ns. The calorimeter offers a quality resolution stemming from electrons and photons, for not wear out its energy resolution the calorimeter is located inside the solenoid. As show Figure 3-5 the electromagnetic calorimeter is organized in Barrel ECAL (EB) and Endcap ECAL (EE), these will be described below.

In the range below 25 to 500 GeV, the ECAL and energy resolution can be describe as

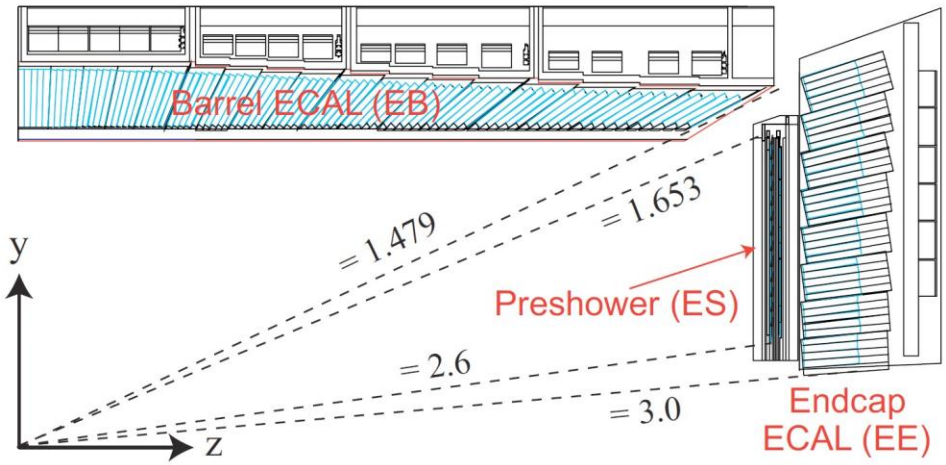

Figure 4-5.: Longitudinal view of a quadrant of electromagnetic calorimeter

the squared sum of three independent terms:

$$\left(\frac{\sigma_E}{E}\right)^2 = \left(\frac{S}{\sqrt{E}}\right)^2 + \left(\frac{N}{E}\right)^2 + C^2 \qquad (4\text{-}1)$$

Taking into account that E denotes the particle energy, the first $\left(\frac{S}{\sqrt{E}}\right)^2$ is referred to as stochastic term which allows parameterize the effects of shower containment and fluctuations Within the second term N is the electric noise and C is a constant term.

The Barrel Calorimeter

The barrel part consider a pseudorapidity $|\eta| < 1.479$ and made up approximately 61 200 crystals covering a volume of 8.14 m^3 while each single crystal is a square with a length 230 mm and cross-section of 22 × 22 mm^2. The granularity of the calorimeter is $\Delta\eta \times \Delta\varphi$ = 0.0175 × 0.0175.

The Endcap Calorimeter

The ECAL contain two endcaps located on the outside part designed to cover a pseudo-rapidity range of 1.48 to 3.0. Each endcap is set up to 10 764 crystals with a volume of 1.52m^3. The crystals have 24.7 × 24.7 mm^2 square with 220 mm of length with a granularity maximum value of $\Delta\eta \times \Delta\varphi$ = 0,05 × 0,05.

4.2.4. Hadronic calorimeter

The Hadronic Calorimeter (HCAL) [18] is a subsystem of CMS calorimeter, which in combination with the ECAL calorimeter and muon system are fundamentals for measure energy

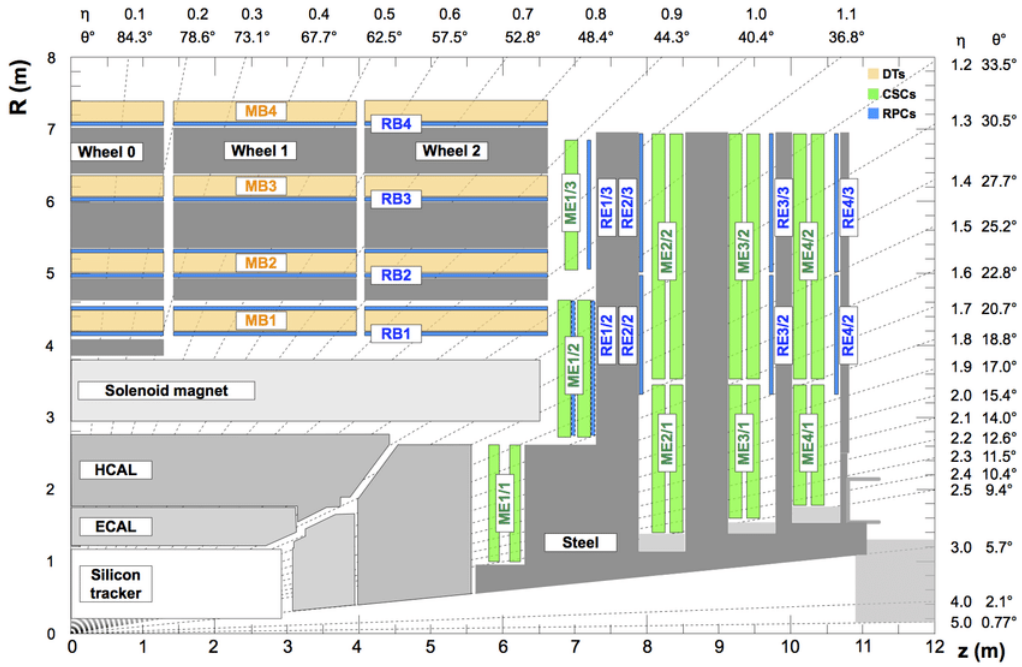

Figure 4-6.: Longitudinal view of Hadronic Calorimeter showing of the hadron barrel (HB), endcap (HE), outer (HO) and forward (HF) calorimeter

and direction of hadron jets or measuring the missing transverse energy due to exotic particles. The HCAL consist of four principal parts: Hadron Barrel (HB), Hadron Endcap (HE), Hadron Outer calorimeter (HO) and Hadron Forward calorimeter (HF) Figure 3 6.

The HB is built up with 36 identical azimuthal wedges covering the region $|\eta| < 1.3$, this is sectioned into two half-barrel sectors inserted between ECAL and the solenoid. The HE covers the pseudorapidity range $1.3 < |\eta| < 3.0$ and has the ability to detect about 34 % of the particles of the fi states. The HB and HE provide a rough idea of hadron showers, in order to increase the detection resolution are added scintillations layers are introduced outside of the detector, this corresponds to the HO and covers a range $|\eta| < 1.3$. The HF has the ability to identify and reconstruct forward jets in addition to enhancing the measurement of missing transverse energy with a range of $3.0 < |\eta| < 5.0$.

The resolution energy is $\sigma/E \sim 65\,\% \sqrt{E} \oplus 5\,\%$ in the barrel, $\sigma/E \sim 85\,\% \sqrt{E} \oplus 5\,\%$ in the endcaps and $\sigma/E \sim 100\,\% \sqrt{E} \oplus 5\,\%$ in very forward calorimeter.

4.2.5. The Muon system

Since muons acquiere large penetration power as compared to others charged particles. They travel through the material almost without any radiative loss. For that reason the CMS muon system is positioned at the outermost edge of the detector. The muon system [20] provides

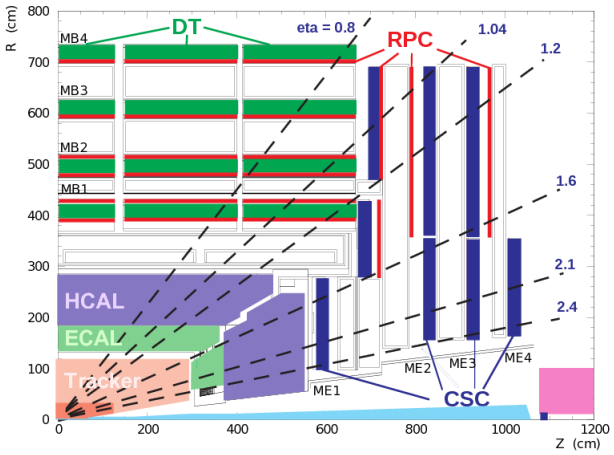

Figure 4-7.: Longitudinal view of a quarter of the muon system

a quality muon identification and reconstruction of its momenta. Inside the solenoid a 4 T magnetic field is generated while in the outer muon system magnetic field is 1-2 T. The pile-up from soft hadrons are reduced by a magnetic field, it allows precision tracking in the silicon detector [34].

In order to obtain the best response of trigger, the signal coming from Drift Tubes and Cathode Strip Chambers provide muon candidates that are reconstructed from hits register in Resistive Plate Chambers, these three differet detectors are used for identify and measure muons Figure 3-4, a general idea of each detector is shown below:

- **Drift Tubes** The Drifts Tubes (DT) are the main muon detector in the barrel region ($|\eta|$ <1.3). The muon chambers are located outside the coil in 12 sectors each sector has four chambers from inside to outside, obtaining a total amount 240 muon chambers which made up the DT chambers [40]. The chambers are held responsible for determinate a muon vector in space through three Super Layers (SL); two SLs outer provide the measurement of the coordinate φ (φ *SL*), while the last SL measures the track coordinate along z-axis (*z SL*) [20].

- **Cathode Strip Chambers** The Cathode Strip Chambers (CSCs) are concentric to the beam line, this subdetector is made of trapezoidal modules mounted on the yokes and was designed for cover up until $|\eta|$ <2.4. The chambers are sectioned in four regions ME1, ME2, ME3 and ME4, where ME stand for ”Muon Endcap”[27]. Due to high the magnetic field and high particle rate thorough endcap, the CSCs are adequate to provide space and time information [20].

- **Resistive Plate Chambers** Resistive Plate Chambers (RPCs) are made of two parallel plates of bakelite. It is placed in barrel and endcap region. It is consist of 480 rectangular shaped barrel chambers, made up of 68136 strips with a total area of 2285m^2. The RPCs provide additional sensitive for trigger system [25].

All chambers have been performed considering all design specifications provided by LHC, the table **4-1** show the properties and statistics of the chambers.

Detector	Drift Tubes	Cathode Strip Chambers	Resistive Plate	
Function	Tracking p_T trigger	Tracking p_T trigger	Resolve tracking ambiguities p_T trigger	
$\|\eta\|$regions	0.0 - 1.3	0.9 - 2.4	0.0 - 2.1	
Stations	4	4	Barrel 6	Endcap 4
Chambers	250	540	360	252
Time resolution	5 ns	6 ns	3ns	

Table 4-1.: Chambers descriptions and properties [20]

4.2.6. The Trigger system

In the LHC collider, the proton bunch crossing occurs at the rate of 40 MHz. It is impossible to incorporate all this amount of data and only a small fraction can be stored for later offline analysis. The goal of CMS trigger [23] is reduce to an acceptable rate of data, in order to perform the reduction of the rate two-step trigger are established, the Level 1 and the High Level Trigger (HLT).

Event selection in Level 1 (L1) [24] trigger is based on information on calorimeter and muon chambers, L1 performs initial rate reduction to 100 kHz before passed on to HLT in a 3.2μs response time. In order to achieve a high resolution for the challenging scatterings, the trigger should be able to register leptons and jets with a range of $|\eta| < 2.5$, nevertheless for single leptons is required an efficiency of 95 % with a threshold of $p_T > 40$ GeV and for dilepton a $p_T > 20$ and 15 GeV. Similar performance is set up for photon and photon triggers besides that jets and multi jets triggers should be over a range $|\eta| <5$ allowing reconstruct the jet spectra overlapping with lower energy data, finally the missing energy is surrounding 100 GeV threshold.

As stated above, calorimeter and muon system are capable of analyzing and collect data locally that subsequently passed to Data Acquisition System (DAQ). The ECAL, HCAL and HF constitute the Trigger Primitive Generator, which affords a synthesized information that will feed to the Regional Calorimeter Trigger so as to reconstruct jets, leptons and photons. The energy and positions registered are raw measurements which are deposited in Global Calorimeter Trigger (GCT), for reconstructing missing segments the Global Muon Trigger is implemented allowing remove fakes and solving ambiguities. Finally, the tidy information is passed to the Global Trigger where the missing transverse energy is estimated and ready for go through HLT trigger.

The High Level Trigger [9] selection is based in software running selection on a cluster of commercial 2000 CPU's. In order to reconstruct an event, several stages have to follow using all information available provides by L1 trigger. First, a local reconstruction is carried out, subsequently to incorporate information from complex algorithms allowing to complete the process.

5. Event reconstruction and simulation

5.1. Particle Reconstruction

The collisions in High Energy Particles give rise to many uneatable, short lived particles which decay spontaneously. However, only the electron, muons, photons and hadrons are the only measurable particles a the detector. They are reconstructed with Particle Flow (PF) algorithm. On the other hand the information about jets and other physics objects can be extracted through stable PF objects. As general idea, the particle identification and reconstruction is establish according to specific characteristics and full information form diff t sub-detector or collection of sub-detectors. For instance, the tracker system, it has the faculty of record trajectories of charge particles, and it can provide a high quality resolution of momenta and direction measures of each particle. Furthermore, the combined information from ECAL, HCAL and tracker system give us the possibility of reconstruct electrons, muons, photons and hadrons. However, exist some particles that feebly or defin i tively are not interacting with the detector, those kind of particles are identified by looking at the missing information, such as missing transverse energy which is defined as:

$$E_T^{miss} = -\sum_i P_T^i \tag{5-1}$$

where the term P_T^i correspond to the transverse momentum of $n-th$ PF object.

Is important to mention that the tracker plays an important role in the reconstruction of the charge particles, thanks to its extraordinary low transverse momentum resolution. Nevertheless, the principal goal is to obtain a high efficiency, through the reduction of fake reconstruct objects. This task is developed using an iterative algorithm, which at the beginning impose a tight selection criteria, giving us a negligible fake rather but a lower efficiency. In order to decrease this, is necessary to implement looser selection yields in throwing fake event but increasing the overall tracking efficiency.

Another key of information implemented to determinate the PF objects is the ECAL and HCAL cluster. Their information give rise to perform several measurements via colorimeter clustering algorithm. For this, the reconstruction of electrons and charged hadrons, energy and direction of photons and neutral hadrons is possible.

5.2. Monte Carlo event generation

The Monte Carlo (MC) generation is regularly used in experimental and theoretical particle physics. Particularly, this tool is fully implemented in predictions of collider experiments, even more it helps in simulate backgrounds models to explore new physics. In collider experiments we look for new physics signatures through of excesses in data over the continuously falling background.

In general, the SM backgrounds can be modeled in two different ways. In the first one, we use events exclusively from simulation and the second by combining simulation and data driven techniques. After the background simulation is necessary to apply scale factors, which are measured using data and often referred as weights. The weights include corrections, such as QCD, electroweak, physics objects identifications and reconstructions scale factors.

An overview the SM simulation is divided in two sections. Firstly, the particle modeling based on collision event, without looking at infractions of particles with the detector. Secondly, now is necessary take in account the response of the detector while modeling particles production in the collision.

The CMS physicists use a variety of tools to generate MC simulations. Some of them corresponds to PYTHIA, MADGRAPH, Sherpa and POWHEG. These softwares share the same basic principles. From each colliding beam, only proton's parton takes parton in the scattering while carrying a fraction of total energy of proton energy. The momentum is calculated probabilistically by random samplings form the parton distribution functions (PDFs). After this, the hadronization process is implemented. It consists in simulate the fragmentation and decays of the initial particles in order to get the final stable particles.

In this analysis, the samples generation are given to an official full simulation of a CMS-like detector to simulate the particles and sub-detectors interactions (under CMSSW 8_0_29)). This is going to be examined in detail in chapter 6.

5.3. GEANT detector simulation

After the MC event generation, the detector response is simulated. The GEANT physics model handle the particle's interaction with the detector itself. GEANT is a software package which includes complete digital representation of the CM detector. The detector definition requires the representation of its geometrical elements, their materials and electronics properties [43].

In general, this software simulate each stable particles passing through the detector, and determine their interaction with the detector in a probabilistic approach. The simulation features are the energy of the particles, the material in the particle is and the magnetic

field. The full GEANT simulation is not 100 % efficient. It requires measuring the CMS calibrations. This calibrations should be included in the simulation set up in order to increase its response.

5.4. PANDA Root

In autumn 2006 the PANDA (Anti-**P**roton **AN**nihilations at **DA**rmstadt) [47] collaboration created a new simulation framework, called PandaRoot. It is based in FairRoot framework, which is strongly supported at GSI. It is built on ROOT and Virtual Monte Carlo. PandaRoot is supported by various C++ compilers and several Linux distributions. PandaRoot is consider as next-generation computing framework. It provide us a fully simulation, reconstruction and analysis. Various particle generator are employed for different physics channels, as well as diff t transport engines to simulate a realistic detector response. The simulated events are based in advanced state and improvements of tracking, also PID algorithms are in development. To summarize, PandaRoot is a versatile and a portable framework for simulation and analysis. The present research is built under this software framework. Our framework is constituted by four differents parts.

- **PandaPro**: Package of productions of PANDA form CMSSW.
- **PandaTree**: contains the panda data format and the tools to create and extend the c++ library for the format. The writing format is fully based in C types and arrays, which means that it is slim, fast to read and write. The library defin e the interface which constructs C++ objects from this tree.
- **PandaCore**: A set common tools on which several of the analysis packages depend. In general it has some core utilities for dealing with ROOT and python. We consider this as the hearth of our analysis.
- **PandaAnalysis**: implements the all analysis set up. Most all our interactions takes place here. There is a core analysis tool, called PandaAnalyzer, that outputs a data format (GeneralTree). PandaAnalyzer is configured using in Analysis class, which can turn on and off analysis specific calculations and corresponding branches in the output tree. The functions are implemented PandaAnalysis/Flat/src/Modules*cc. and the specific analysis for leptonic monotop is located in PandaAnalysis/LeptonicMonoTop.

5.5. Physics Objects

This chapter includes detailed information about all main physics objects used in this analysis. The Physics Object Group (POG) recommendations are mostly followed. Nonetheless,

some particular variations had been considered in our favor. The physics objects and selection are described as follow:

Primary vertex and pile-up reweighing

The proton-proton collision that take place in the LHC causes a several interactions appear inside the same bunches crossing, this is know as pile-up. However, pile-up of greater than 25. That presents a challenge to the CMS tracker. The pile-up reweigh is performed in order to reweight the true number of pile up interactions in MonteCarlo. The events are selected by applying loose selection cuts and vertex associated to largest p_T sum of member tracks.

Jets

This analysis employed an AK4 jets algorithm. The reconstruction of jets is performed by clustering the PF candidates in an event using the anti-k_t algorithm is implemented [41] with ΔR=0.4, where $\Delta R = \sqrt{\Delta\eta^2 + \Delta\varphi^2}$, η being the azimuthal angle with respect to the beam direction. In order to ovoid consider specific jets, the Ak4 are requiring at least jets bigger than 25 GeV and $|\eta| < 2.5$. Loose jet identification recommendations are used from jet-met POG. However, the resolution of jet in the simulation do not fully reproduce the observe resolution in the data, for this reason the p_T resolution of jets is corrected in simulation following the correction from [26].

B-tagged Jets

Jets stemming from b quarks are identified using a secondary-vertex-tagging algorithm (CSV) [14]. The identification of b jets is important to suppress the backgrounds. The b jets are tagged using BTV POG recommended medium working pint of bigger than 0.80. The b jet are selected with $p_T > 25$ GeV and $|\eta| < 2.5$.

Muons and electrons

Muons and their identification

The main backgrounds are electroweak process involving muons as the outcome particles. It is crucial identify muons in the signal region to be able to eliminate the background contribution. Muon can be reconstructed as a global or tacker muon. Particularly, this analysis implement a GlobalMuon algorithm and since the momentum resolution is dominated by the inner tracking system for $p_T < 200$ GeV, the inner track momentum is used as an estimator of the muon momentum. The selections are recommended by the POG. Loose muons

are identified by means of the POG-defined Loose working point. For medium muons mini-isolation must be less than 0.1, and for loose muons mini-isolation must be less than 0.4. Muons are subject to the tight selections. This guarantee that the muon to be well isolated and have a similar p_T measurement in the inner detector and muon spectrometer.

Electrons and their identification

In this study the electron reconstruction and identification efficiencies are measured in order to study signal. Electrons are reconstructed starting from the reconstruction in the silicon detector with a cluster of energy in the ECAL and superclusters (SC) around seed cluster. The superclusters are then matched to trajectory seeds, which are built from pairs or triplets of hits in the inner tracker layers. Based on this track seeds, electron tracks are built by fitting the trajectory with a Gaussian-sum filter (GSF) algorithm to estimate the electron track parameters. Electron candidates are built from the association of a GSF track and a supercluster. The ECAL fiducial region is defined by $|\eta_{SC}|$ <1.4442 (barrel) or 1.566< $|\eta_{SC}|$ <2.5 (endcap), where $|\eta_{SC}|$ is the pseudo-rapidity of the supercluster.

The selection requirements for the electron in order to suppress the background process, is p_T > GeV and $|\eta|$ < 2.5.

6. Data and Monte-Carlo Samples

This study is based on the full 13 TeV datasets of a total integrated luminosity of 35.9fb^{-1} recorded in 2016. The analysis presented here has been carried out using the CMS official software framework for event generation, simulation and reconstruction. Data events have been registered during the 2016 data taking campaign from proton-proton collisions at a center-of-mass energy of 13 TeV. Monte Carlo events have been produced by caring about reproducing faithfully the conditions of this data taking. Monte Carlo as well as data samples have been processed and analyzed within CMSSW 8 0 29 release.

6.1. Dataset

The analysis is based in a complete dataset recorded in 2016, corresponding to a total integrated luminosity of 35.9 fb^{-1}. The data has been certified with the golden JSON fi Cert_271036-284044_13TeV_23Sep2016ReReco_Collisions16_JSON.txt, corresponding to runs 271 036 – 284 044.

Dataset Name	Integrated luminosity (fb^{-1})
/SingleElectron/Run2016B-03Feb2017_ver2-v2/MINIAOD	5.764
/SingleElectron/Run2016C-03Feb2017-v1/MINIAOD	2.566
/SingleElectron/Run2016D-03Feb2017-v1/MINIAOD	4.227
/SingleElectron/Run2016E-03Feb2017-v1/MINIAOD	4.009
/SingleElectron/Run2016F-03Feb2017-v1/MINIAOD	3.094
/SingleElectron/Run2016G-03Feb2017-v1/MINIAOD	7.514
/SingleElectron/Run2016H-03Feb2017_ver2-v1/MINIAOD	8.310
/SingleElectron/Run2016H-03Feb2017_ver3-v1/MINIAOD	0.215
/SingleMuon/Run2016B-03Feb2017_ver2-v2/MINIAOD	5.784
/SingleMuon/Run2016C-03Feb2017-v1/MINIAOD	2.573
/SingleMuon/Run2016D-03Feb2017-v1/MINIAOD	4.248
/SingleMuon/Run2016E-03Feb2017-v1/MINIAOD	4.008
/SingleMuon/Run2016F-03Feb2017-v1/MINIAOD	3.102
/SingleMuon/Run2016G-03Feb2017-v1/MINIAOD	7.540
/SingleMuon/Run2016H-03Feb2017_ver2-v1/MINIAOD	8.391
/SingleMuon/Run2016H-03Feb2017_ver3-v1/MINIAOD	0.215

Table 6-1.: Summary of official datasets

6.2. Backgrounds

The backgrounds events are taken form the CMS Monte Carlo production performed with the full simulation of the realistic detector conditions. The main background samples correspond to $t\bar{t}$+jets and W+jets process, which have been generated using MADGRAPH 5[7], interfaced to PYTHIA 8 [45] for the hadronization of quarks and TAUOLA [2] for the decay of τ. In order to increase the available MC statistics of the important W+jets sample, the MC events are produced exclusively for additional partons ranging from 1 to 4. The MADGRAPH production for W+jets without any addition parton at the matrix element level is constructed from the inclusive W+jets by selecting the W+jets processes using the event process ID. The corresponding cross-section is determined by simply subtracting the exclusive sample cross-sections to the inclusive one. The sub-dominant di-bosons samples are produced with pythia 8. Single top (tW channel) samples are produced with the POWHEG [35] generator interfaced with HERWIG [33] for the hadronization of quarks.

Is convenient to give a brief description of the backgrounds, in order to mention the generation description of each process.

- **$t\bar{t}$** : Particularly, for monotop analysis, we split the $t\bar{t}$ into two processes. One of them considering events with one lepton, and the other with two lepton. Called $t\bar{t}$ di and single-lepton respectively. However, for both processes the MC samples for having been generated using aMC@NLO and Powheg generators at next-to-leading-order (NLO).

- **W + jets** and **Z + jets** : The MC samples for $W(R\nu)$+jets and Z_{RR} have been generated through MadGraph at leading order (LO) in QCD in several H_T bins.

- **Single top:** The MC samples events have been produced with Powheg generator at NLO.

- **Diboson:** Monte Carlo samples for WW, ZZ and WZ have been generated through Pythia 8 at LO.

- **QCD:** The QCD Monte Carlo samples have been generated using the MadGraph at leading order in QCD in several H_T bins.

These processes are simulated and are shown in the Tab.**6-2**. It contains the cross section and the dataset name for each physics process.

Process	Dataset name	σ (pb)	Order
$t\bar{t}$	/TTJets DiLept TuneCUETP8M1 13TeV-madgraphMLM-pythia8	85.17	NLO
	/TTJets SingleLeptFromTbar TuneCUETP8M1 13TeV-madgraphMLM-pythia8	180.99	NLO
	/TTJets SingleLeptFromT TuneCUETP8M1 13TeV-madgraphMLM-pythia8	180.99	NLO
W($l\nu$)+ jets	/WJetsToLNu HT-100To200 TuneCUETP8M1 13TeV-madgraphMLM-pythia8	1343	LO
	/WJetsToLNu HT-200To400 TuneCUETP8M1 13TeV-madgraphMLM-pythia8	359.6	LO
	/WJetsToLNu HT-400To600 TuneCUETP8M1 13TeV-madgraphMLM-pythia8	48.85	LO
	/WJetsToLNu HT-600To800 TuneCUETP8M1 13TeV-madgraphMLM-pythia8	12.05	LO
	/WJetsToLNu HT-800To1200 TuneCUETP8M1 13TeV-madgraphMLM-pythia8	5.501	LO
	/WJetsToLNu HT-1200To2500 TuneCUETP8M1 13TeV-madgraphMLM-pythia8	1.329	LO
	/WJetsToLNu HT-2500ToInf TuneCUETP8M1 13TeV-madgraphMLM-pythia8	0.03216	LO
	/WJetsToLNu HT-70To100 TuneCUETP8M1 13TeV-madgraphMLM-pythia8	1319	LO
Single Top	/ST t-channel antitop 4f inclusiveDecays 13TeV-powhegV2-madspin-pythia8 TuneCUETP8M1	80.95	NLO
	/ST tW top 5f inclusiveDecays 13TeV-powheg-pythia8 TuneCUETP8M1 ext1-v1	35.85	NLO
Z(ll)+ jets	/DYJetsToLL M-50 HT-100to200 TuneCUETP8M1 13TeV-madgraphMLM-pythia8	148.0	LO
	/DYJetsToLL M-50 HT-1200to2500 TuneCUETP8M1 13TeV-madgraphMLM-pythia8	0.1514	LO
	/DYJetsToLL M-50 HT-200to400 TuneCUETP8M1 13TeV-madgraphMLM-pythia8	40.94	LO
	/DYJetsToLL M-50 HT-2500toInf TuneCUETP8M1 13TeV-madgraphMLM-pythia8	0.003565	LO
	/DYJetsToLL M-50 HT-400to600 TuneCUETP8M1 13TeV-madgraphMLM-pythia8	5.497	LO
	/DYJetsToLL M-50 HT-600to800 TuneCUETP8M1 13TeV-madgraphMLM-pythia8	1.367	LO
	/DYJetsToLL M-50 HT-70to100 TuneCUETP8M1 13TeV-madgraphMLM-pythia8	175.3	LO
	/DYJetsToLL M-50 HT-800to1200 TuneCUETP8M1 13TeV-madgraphMLM-pythia8	0.6304	LO
Diboson	/WW TuneCUETP8M1 13TeV-pythia8	118.7	NLO
	/WZ TuneCUETP8M1 13TeV-pythia8	47.13	NLO
	/ZZ TuneCUETP8M1 13TeV-pythia8	16.523	NLO
QCD	/QCD HT1000to1500 TuneCUETP8M1 13TeV-madgraphMLM-pythia8	1064	NLO
	/QCD HT100to200 TuneCUETP8M1 13TeV-madgraphMLM-pythia8	27990000	NLO
	/QCD HT1500to2000 TuneCUETP8M1 13TeV-madgraphMLM-pythia8	121.5	NLO
	/QCD HT200to300 TuneCUETP8M1 13TeV-madgraphMLM-pythia8	1735000	NLO
	/QCD HT300to500 TuneCUETP8M1 13TeV-madgraphMLM-pythia8	366800	NLO
	/QCD HT500to700 TuneCUETP8M1 13TeV-madgraphMLM-pythia8	29370	NLO
	/QCD HT50to100 TuneCUETP8M1 13TeV-madgraphMLM-pythia8	278700000	NLO
	/QCD HT700to1000 TuneCUETP8M1 13TeV-madgraphMLM-pythia8	6524	NLO
	/QCD HT2000toInf TuneCUETP8M1 13TeV-madgraphMLM-pythia8	25.42	NLO

Table 6-2.: Summary of official Monte Carlo samples used for background studies. All Monte Carlo samples have been processed with pile-up scenario consistent with Summer16 production

6.3. Generation of signal events

Signal events are generated through a private production. First the LHE fi are produced with the MADGRAPH 5 generator [7](version 1.5.3 under CMSSW_8_0_29). The monotop model, described in Sec. 3, is implemented in MADGRAPH by means of the FeynRules [1, 10, 6] program. The showering of extra jets and the hadronization are then performed by the PYTHIA 8 [46] software (version 8.175 under CMSSW_8_0_29). For the case of FCNC, vector invisible particles are considered, while in the case of the resonant production mode, the resonant particle is a scalar and the invisible particle is a fermion (Sec. 3). The coupling strength is by default set to a =0.1, but as the signal cross section evolves as a^2, it can then be re-scaled to different values of a.

Various mass points are considered depending on the production mode, through fla vor-changing neutral current V. The table **6-3** contain all 32 samples that have been simulated for leptonic monotop signal. The M_V denoted the mass of the bosonic mediator with spin-1 (figure **3-1**). While M_{DM} denotes the mass of dark matter particle candidate.

	Mediator $\mathbf{M_V}$ **[GeV]**	Particle $\mathbf{M_{DM}}$ **[GeV]**			
Vector_MonoTop_Leptonic_NLO	**2500**	1000	500	200	1
Vector_MonoTop_Leptonic_NLO	**2000**	1000	990	200	1
Vector_MonoTop_Leptonic_NLO	**2250**	1000			
Vector_MonoTop_Leptonic_NLO	**1750**	1000	500	200	1
Vector_MonoTop_Leptonic_NLO	**1500**	1000	500	200	1
Vector_MonoTop_Leptonic_NLO	**1000**	1000	490	200	1
Vector_MonoTop_Leptonic_NLO	**750**	1000	500	200	1
Vector_MonoTop_Leptonic_NLO	**500**	1000	500	200	
Vector_MonoTop_Leptonic_NLO	**300**	1000	500	200	1

Table 6-3.: Mass point of DM particle in relation with mediator V

7. Event Selection

In order to probe the leptonic monotop channel, we focus mainly on the strategy in the reconstruction of the leptonically decaying of top quark motivated by the fact that this signature is cleaner than the hadronic mode. The events of interest involve the presence of one jet tagged as result of b-quark in association to W boson with a final leptonic state, reconstructing signatures with this rather particular structure is challenging due to the QCD multijet backgrounds.

This chapter is completely dedicated to carrying out a general check of some relevant variables of this analysis. This will allow us to establish appropriate cuts. All the graphs presented below are correctly normalized. The normalization is related to generation samples. This means that normalization need consider the weights, which are associated with generated MC events.
In general, the normalization is stablish by:

$$N = \frac{\sigma \cdot \text{mcWeight} \cdot \text{Lumi}}{\text{number of simulated events}} \tag{7-1}$$

where the σ denoted the cross sections. All process with their respectively cross sections were mentioned in table **6-2**. The *mcWeight* corresponds to the weights of MC events. The weights are saved into the tree. On the other hand, the *Lumi* denotes the integrated luminosity. Particularly, we use an integrated luminosity of 35.9fb^{-1}. Finally, the *number of simulated events* is established into the generation of MC events.
It is important to mention that to carry out the calculations in a simple way, the variable *normalizedWeight* is defined into the tree. It is defined by

$$\textit{normalizedWeight} = \frac{\sigma \cdot \text{mcWeight}}{\text{number of simulated events}} \tag{7-2}$$

It means, that the normalization into our selection script just will be described by:

$$N = \text{normalizedWeight} \cdot \text{Lumi} \tag{7-3}$$

The selection script is located in the Appendix A, while the plotting script is in Appendix B.

7.1. Discussion and cuts

This section includes the set of criteria, used to select events in signal region. We will analyze a total of 31 signal and 7 backgrounds ntuples. They were listed in section 6. As a fi step all the signs were plotted together, in order to analyze relevant kinematic variables. Specifically, the Fig. **7-1** present the missing transverse energy (a) and transverse mass distribution (b) for several masses of mediator V and DM particles. The peak in $\not{E}^{miss}_{T}$ distribution is a shape that we were expecting in the signal. Something relevant in this plot is that we can noticed that the peak is located in 200 GeV. This fact will be useful when we will establish cuts. On the other hand, the M_T distribution is the main variable that we are looking for. For that reason, it is important to analyze it from the beginning. Keep an eye on this variable will help us understand and verify our analysis. Furthermore, it easily identifies a clearly peak at 300 GeV.

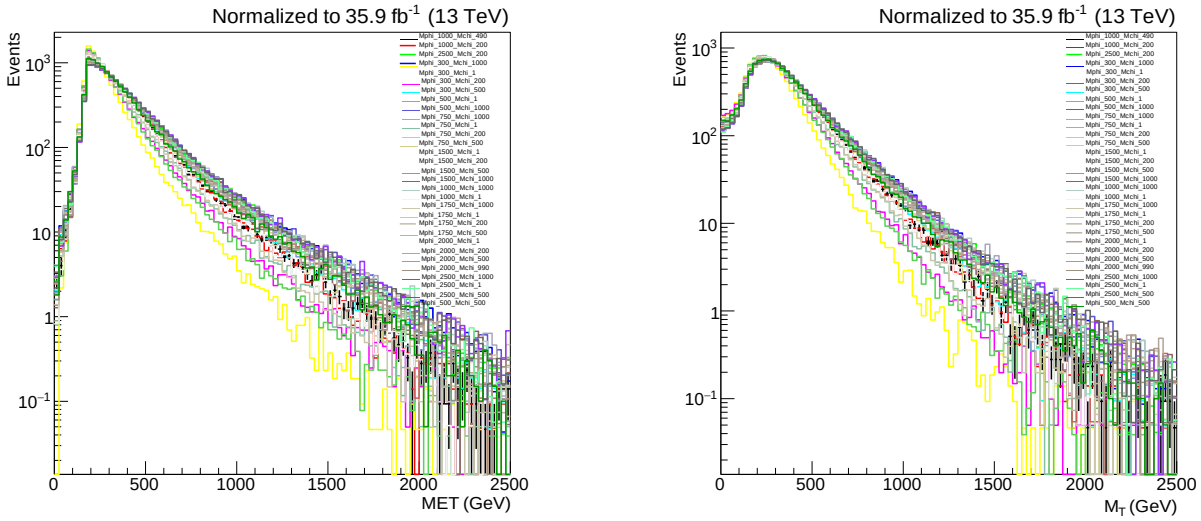

(a) (b)

Figure 7-1.: Comparison between all 31 signal samples for a) missing transverse energy (MET) and b) transverse mass (M_T)

Taking into account the previous graphs, we selected only four signal samples (table **7-1**). These were chosen conveniently, this means that we focus on the more dramatics signal samples. This will help us see how signal behaves in each case.

After the signal samples are selected, it is convenient to compare these with all the backgrounds. The figure **7-2** show us the $\not{E}^{miss}_{T}$ and M_T distributions. According to the $\not{E}^{miss}_{T}$ distribution, we can affirm that is consistent with we were expecting. Furthermore, if we

	Mediator $\mathbf{M}_V$ **[GeV]**	Particle $\mathbf{M}_{DM}$ **[GeV]**
1	**2500**	1000
2	**1000**	200
3	**300**	200
4	**300**	1

Table 7-1.: Selection of main signal samples

focus in a range between 0 and 200 GeV, we can realize that consider a cut in 200 GeV can be convenient. This will help to exclude regions where the signal shape is lower in comparison with the background's shapes. On the other side, the M_T distribution for signal exhibit a flat shape between 200 and 300 GeV. It is consist with the affirmation in figure **7-1** graphic b). Due to none cut have been applied, it is natural that the backgrounds predominate over the signal.

In general for the two distributions mentioned above the $t\bar{t}$ (di and single-lepton) are the main backgrounds. The second background is the w+jets process. On the other hand, QCD corresponds to lower background but it is not negligible. This consistent with what was mention in subsection 3.2.1.

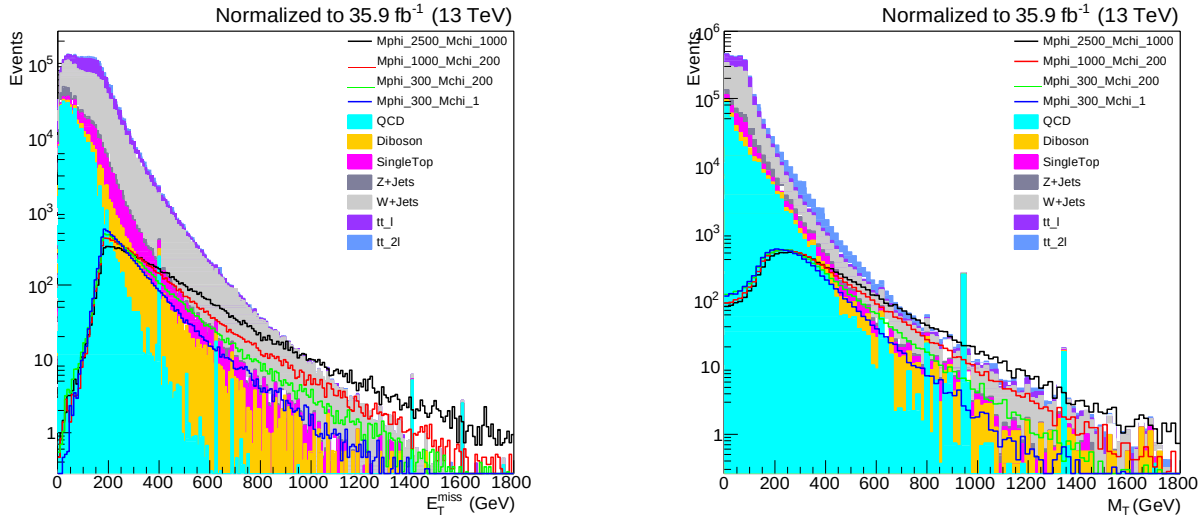

(a) (b)

Figure 7-2.: Comparison between main backgrounds and signal samples for a) missing transverse energy (E_T^{miss}) and b) transverse mass (M_T)

Up to this point, we have not been thinking any cut but we built a general idea by viewing the graphic displays. In this manner now we can go one step further.

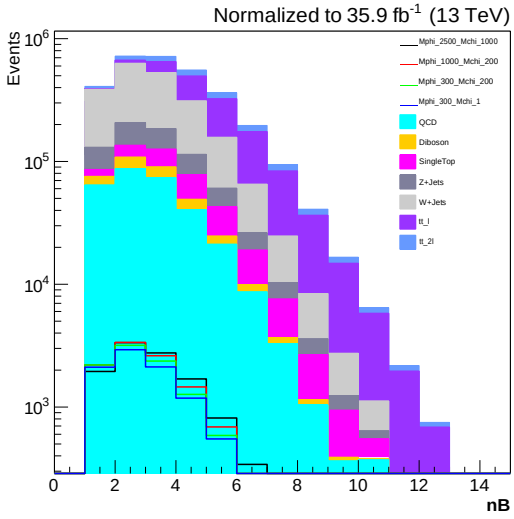

Figure 7-3.: Number of Jets

7.1.1. Object Selection

The object selection is especially focused on a selection of jets and lepton. In general, this idea was described in section 5.5. The required objects for this analysis are what are listed below.

1) nJet > 0
2) jetPt > 25 GeV
3) jetEta < 2.5
4) nTightLep = 1

An important variable that is necessary to analyze is the number of the Jets. The fi **7-3** show us how many jets are present in backgrounds and signal. In order to have a clear idea of the jets and their characteristics, the table **7-2** shows the value of p_T and η for each jet. This information was extracted from the tree.

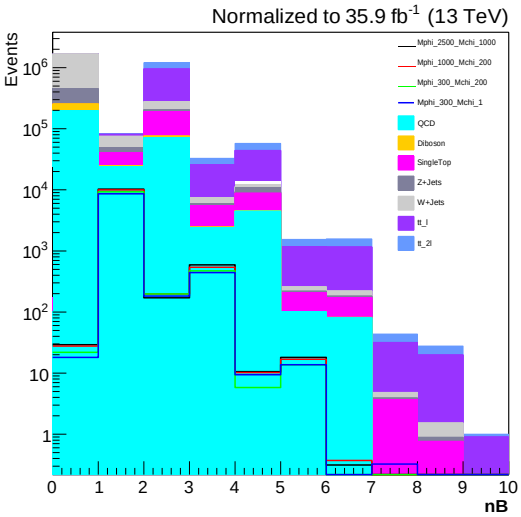

H

Figure 7-4.: Number of b Jets

In summary, the first cuts that we established have been defined in this section. The lepton and jets characteristic that are mentioned above, they will be fully applied in the next section for all signal and background samples.

7.1.2. Base Selection

After object selection, the new cuts will be established according to the final states that we are looking for, such as the number of b jets. The section 3 gave us details about the signal features and their importance. The cuts are establish in the signal region.
Keeping in mind the previous affirmation, we graphed the number of b jets (figure **7-4**). The bigger value for number of b jets of signal is located at one, this is consistent with the figure state of monotop signature. Furthermore, the backgrounds shapes within the same region are lower in comparison with the signal. For the main backgrounds the maximum values make sense. For instance, $t\bar{t}$ (di and single-lepton) it highest value is in two, while for W+Jets background, its higher value is located in cero.

Considering the previous affirmations. The first reasonable cut will take account the number the b jets bigger than cero. This will help us start to restring the analysis in the signal control region. The figure **7-5** present the E_T^{miss} and M_T distributions after the final cut. We can realize that both distribution present a lower background shape if we compare with fi re **7-2**, which are the same distribution but without cuts. However, the signal is immutable as expected.

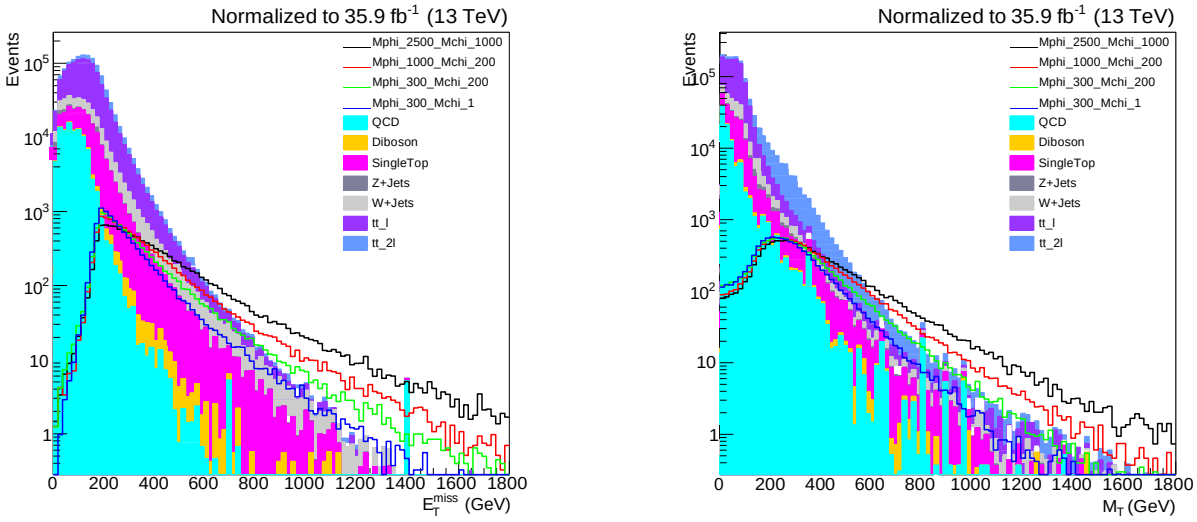

(a) (b)

Figure 7-5.: Comparison of (a) Missing Transverse Energy and (b) Transverse mass after final cut (nB > 0)

In order to get stronger suppression of the backgrounds, the second cut is associated with a cleaner cut at the number of the b jets. Focusing on the signal region we establish the nB =1, as second cut. The figure **7-6** clearly shows the effect of this second cut in the E_T^{miss} and M_T distributions. The signal begins to dominant over the backgrounds.

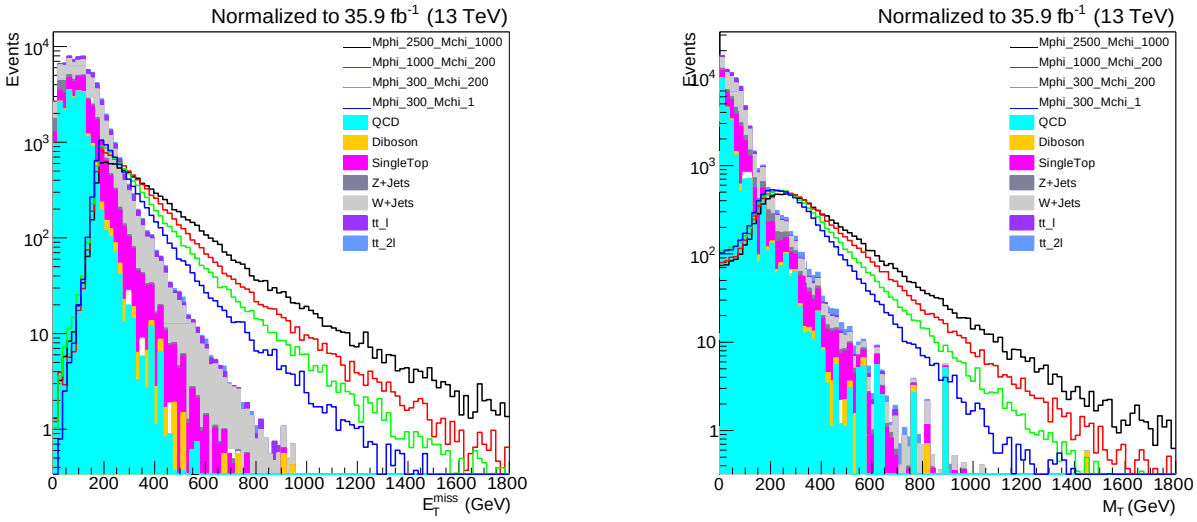

(a) (b)

Figure 7-6.: Comparison of (a) Missing Transverse Energy and (b) Transverse mass after applied the final and second cut (nB > 0 & nB=1)

8. Results

In the section 7 is established the total selection. This is split in object and base selection. After applied all this considerations in E_T^{miss} and M_T distributions, the backgrounds were sufficiently suppressed, and the signal is more prevalent over them. Nevertheless, in order to suppress more the backgrounds is necessary implement a cut around E_T^{miss}. This was mentioned in subsection 7.1. This third cut is for $E_T^{miss} > 200$ GeV.

The expected and observed event yields in monotop signal region after third cut are reported in fi e **8-1**. Particularly, the M_T distribution present interesting results. The signal shapes are clearly predominant over backgrounds. The QCD is almost suppressed, while $t\bar{t}$ (di and single-lepton) and W+jets are not negligible, as main backgrounds should behave.

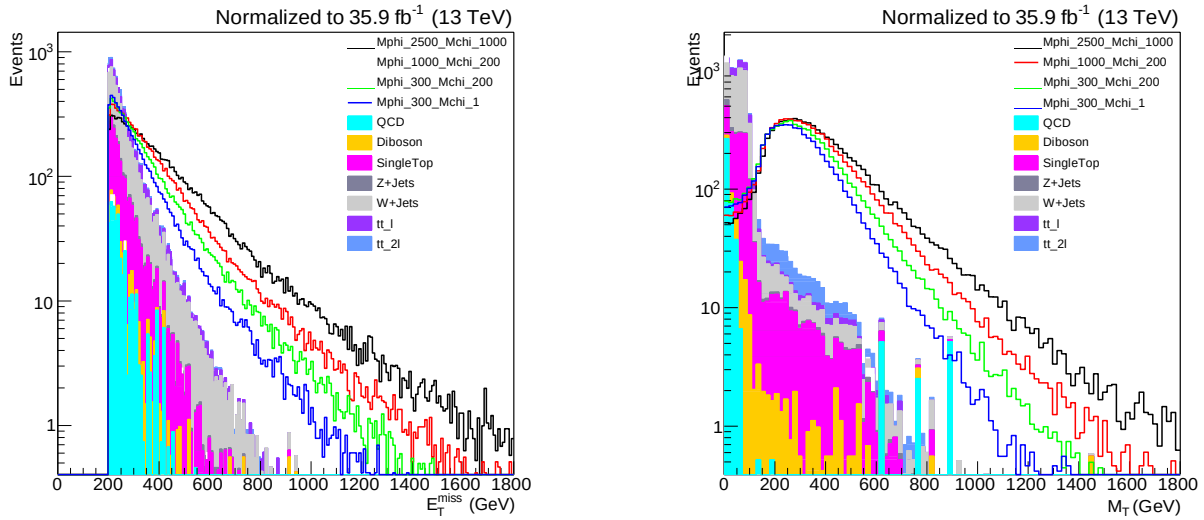

(a) (b)

Figure 8-1.: Comparison of (a) Missing Transverse Energy and (b) Transverse mass after applied the fi and second cut (nB > 0 & nB=1 & $E_T^{miss} > 200$ GeV)

Other main variables corresponding to the P_T and η of muon are defi in Appendix C.

8.1. Cut-Flow

In summarize, we fi among the physical quantities of each event those that are more *discriminant* and we apply cuts on these variables. The selection procedure is a sequence of our cuts, and it is described by a plot that is called Cut-Flow (figure **8-2**). This graph is very clearly the backgrounds are considerably suppressed as the cuts are implemented. Particularly, in the last cut, the signal shows a predominance over the background events, which is consistent with the figure **8-1**.

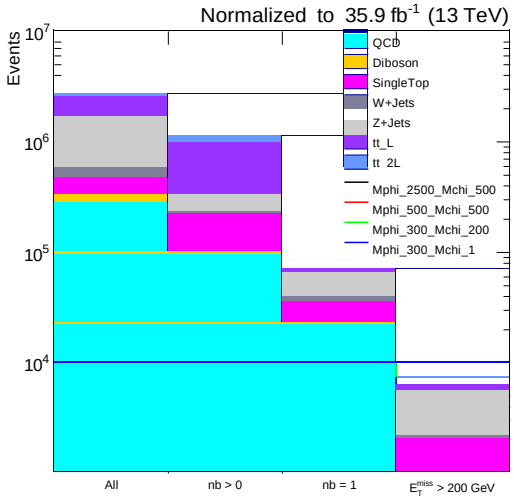

Figure 8-2.: Cut-Flow

The numerical information of yields after each cut, it was registered for . This is very important to double check our considerations because both distributions have to provide the same yields numerical information. This was verified successfully and the yields information is presented in table **8-1**.

		Cut 1 All	**Cut 2** nB > 0	**Cut 3** nB = 1	**Cut 4** $E_T^{miss} > 200$GeV
Backgrounds	*QCD*	284980	95106	22070	402
	Diboson	52276	4643	808	125
	SingleTop	119757	119688	13844	1526
	Z + Jets	101725	10232	3440	121
	W + Jets	1322355	100365	25524	3635
	tt_l	712837	712827	5841	837
	tt_ll	158159	158158	1055	244
Signals	$M^V_{2500}M^X_{1000}$	10832	10804	10032	8676
	$M^V_{1000}M^X_{200}$	10531	10504	9758	8030
	$M^V_{300}M^X_{200}$	9771	9749	9075	7078
	$M^V_{300}M^X_{1}$	9067	9050	8418	6172

Table 8-1.: Numerical information of cut-flow (figure **8-2**)

8.2. Exclusion limits

This section is dedicated to understand an important feature of the analysis in particle physics. In general, the particle physicist have to handle no just the dramatic discoveries but they have to manage no discovery regions. They have to be able to push the limits to the regions with no discoveries are. These are called confidence limits, including a confidence belt.

The figure **8-3** shows a general idea how confidence belt is build. This belt is important to quantify uncertainties on data. Confidence limits are the maximum and minimum values bracketing the statistic of interest (usually the arithmetic or geometric mean) based on the distribution of the data at a certain confidence level (usually 95%). In other words, the confidence limits are the maximum or minimum values above or below which you are confident (at a selected confidence level) that the statistic will occur.

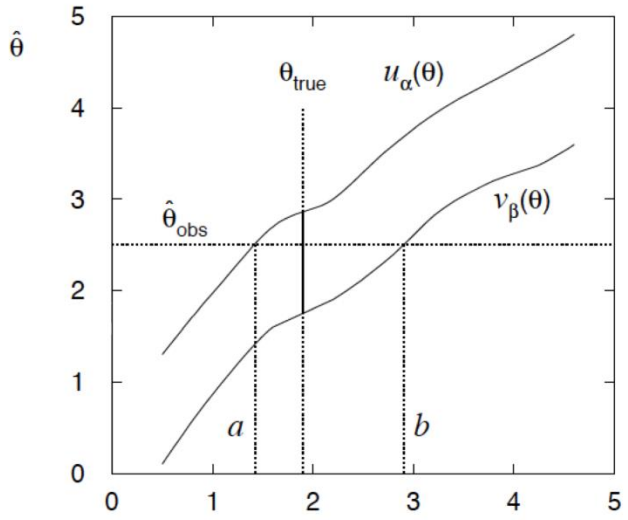

Figure 8-3.: General example of confidence belt

In our case, the figure **8-4** shows the confidence belt of leptonic monotop analysis. This belt is obtained by combinations through the description of the signal and background shapes via analysis configuration files, called datacards. In this case, an example of how they were written can be found in Appendix D.

In figure **8-4** the dotted line represent the expected limit. That means the median value of σ_{DM} which excluded under background-only hypothesis. The green and yellow bands correspond to 68\% and 95\% confidence level intervals, respectively. In our case, the model has one unknown parameter, the DM particle mass. The scaling factor σ_{DM} on the DM cross section is used as second parameter.

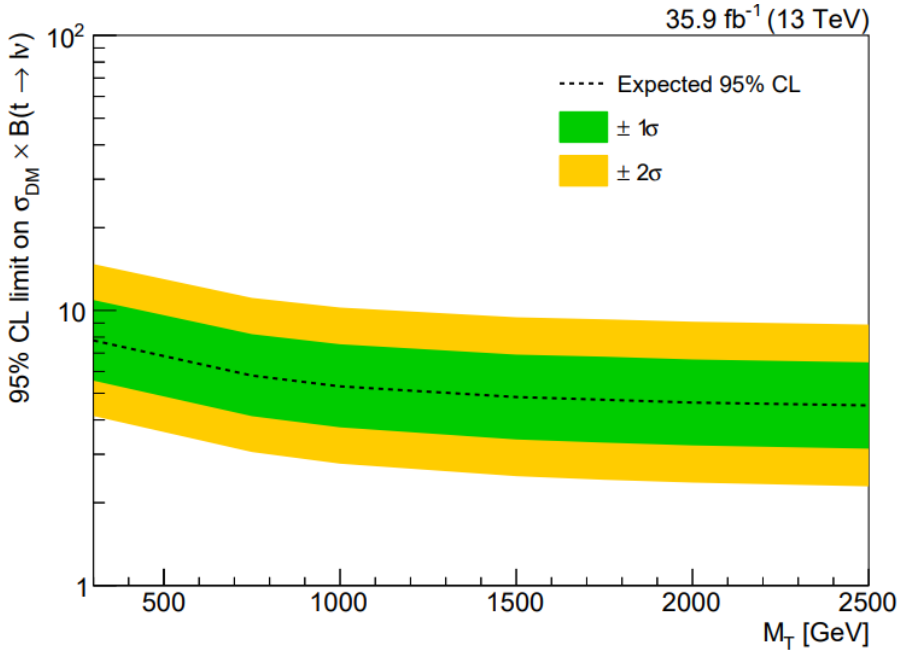

Figure 8-4.: 95 % CL. expected upper limits on the cross section times branching fraction for top production

Particularly, the exclusion limit (figure \ref{exclusion}) shows that the monotop signal with a luminosity of 35.9 fb^{-1} can be excluded in a range between 1000 and 2500 GeV, with a cross section bigger than 6 pb. .

8.3. Conclusion

Understanding the existence and characteristics of dark matter is still an enigma. We learned that the most motivated candidates for dark matter are the WIMPs. However, indirect detection and LHC experiments do not provide any convincing signals of such particles so far. The DM search at LHC is quiet challenging because we don't know how dark matter interacts with ordinary mass. However, dark matter searches at collider experiments have grown interested due to experimental feasibilities that LHC provides. The dark matter models have been devised to predict missing transverse energy signal, such as leptonic monotop channel. It deals with the direct production of dark matter in association with SM states. The leptonic monotop model looks for events with one single lepton, one b-jet and large missing transverse energy, which is one of the main topics of this dissertation.

I performed this analysis by studying and analyzing monotop events in proton-proton collisions at center of mass $\sqrt{S}$= 13 TeV normalized to an integral luminosity of 35.9 1/fb, collected in 2016 of by CMS. I interpreted the results around the main kinematics variables. The main features of this model are $E_T^{miss}$and M_T distributions. After applied all selection criteria we noticed the signal purity over backgrounds. Particularly, the $\bar{t}t$ (di and single-lepton) and w+jets show a dominance over the rest of backgrounds, such as irreducible backgrounds should behave, while the QCD background is suppressed. The Cut-Flow distribution showed the efficiency of each cut and we verified successfully the yields information for $E_T^{miss}$and M_T distributions. Finally, the exclusion limit shows that leptonic monotop signals can be excluded in ranges as [1000, 2500] GeV, with a cross section greater than 6pb.

Clearly, we still have a lot of work to do but I will maintain the hope that one day we can observe a signature.

A. Appendix: Selection script

```
void Selection_MET3(TString file1, TString file2, TString file3, TString file4, TString file5,
TString file6, TString file7, TString file8, TString file9, TString file10, TString file11)

{

  THStack *hs = new THStack("hs","pfmet");

  string objSel = "nJet>0 && jetPt[0]>25 && jetEta[0]<2.5 && nTightLep==1 ";
  string baseSel = "nB>0 && nB==1 && pfmet>200";
  string totSel = "normalizedWeight * ((" + objSel + ") && (" + baseSel + "))";


  TFile f1(file1);
  TTree* t1 = (TTree*) f1.Get("events");
  TH1F* hsig1 = new TH1F("hsig1", "pfmet", 100, 0, 1800);
  t1->Draw("pfmet>>hsig1", totSel.c str(), "goff");
  hsig1->SetDirectory(0);
  f1.Close();
  .
  .
  .
  .
  .
  TFile f11(file11);
  TTree* t11 = (TTree*) f11.Get("events");
  TH1F* htt2l = new TH1F("htt2l", "pfmet", 100, 0, 1800);
  t11->Draw("pfmet>>htt2l", totSel.c str(), "goff");
  htt2l->SetDirectory(0);
  f11.Close();

  TFile fOut("outputpfmet totSel3.root", "RECREATE");
  hsig1->Write();
  hsig2->Write();
  hsig3->Write();
  hsig4->Write();

  hqcd->Write();
  hvv->Write();
  htop->Write();
  hzjets->Write();
  hwjets->Write();
  htt1l->Write();
  htt2l->Write();

  fOut.Close();

  }
```

B. Appendix: Plotting script

```
import ROOT
from ROOT import TLegend, TLatex, TText

ROOT.gROOT.SetBatch()
ROOT.gStyle.SetOptStat(0)
ROOT.gStyle.SetOptTitle(0)

fIn = ROOT.TFile("outputmT_NOCUT_Final.root")

rebin = 5

h_qcd    = fIn.Get("hqcd")
h_vv     = fIn.Get("hvv")
h_top    = fIn.Get("htop")
h_zjets  = fIn.Get("hzjets")
h_wjets  = fIn.Get("hwjets")
h_tt1l   = fIn.Get("htt1l")
h_tt2l   = fIn.Get("htt2l")
h_sig1 = fIn.Get("hsig1")
h_sig2 = fIn.Get("hsig2")
h_sig3 = fIn.Get("hsig3")
h_sig4 = fIn.Get("hsig4")

st = ROOT.THStack()

h_qcd.Scale(35900)
h_qcd.Rebin(rebin)
h_qcd.SetFillColorAlpha(7,0.0937649)
h_qcd.SetLineColor(7)
st.Add(h_qcd)
.
.
.
h_sig4.Scale(35900)
h_sig4.Rebin(rebin)
h_sig4.SetLineColor(4)
h_sig4.SetLineWidth(2)

c = ROOT.TCanvas("c", "c", 800, 800)
c.SetLogy()

st.Draw("HIST")
h_sig1.Draw("SAME_HIST")
h_sig2.Draw("SAME_HIST")
h_sig3.Draw("SAME_HIST")
h_sig4.Draw("SAME_HIST")

st.GetXaxis().SetTitle("M_{T} (GeV)") s
t.GetYaxis().SetTitle("Events")
st.GetYaxis().SetTitleOffset(st.GetYaxis().GetTitleOffset()* 1.3)
st.SetMinimum(1.0)

## legend
leg = ROOT.TLegend(0.6,0.5,0.9,0.9);
leg.AddEntry(h_sig1, "Mphi_2500_Mchi_1000", "l")
.....
leg.Draw("SAME")

def drawCMS(lumi, text, onTop=False):
    latex = TLatex()
    latex.SetNDC()
    latex.SetTextSize(0.04)
    latex.SetTextColor(1)
    latex.SetTextFont(42)
    latex.DrawLatex(0.5, 0.985, "#bf{%s}" %(text))
    latex.DrawLatex(0.90, 0.95, "%s fb^{-1} (13 TeV)" %lumi)

drawCMS(35.9,"")

c.SaveAs("outputmTNOCUTfinal.pdf")
```

C. Appendix: Muon distributions

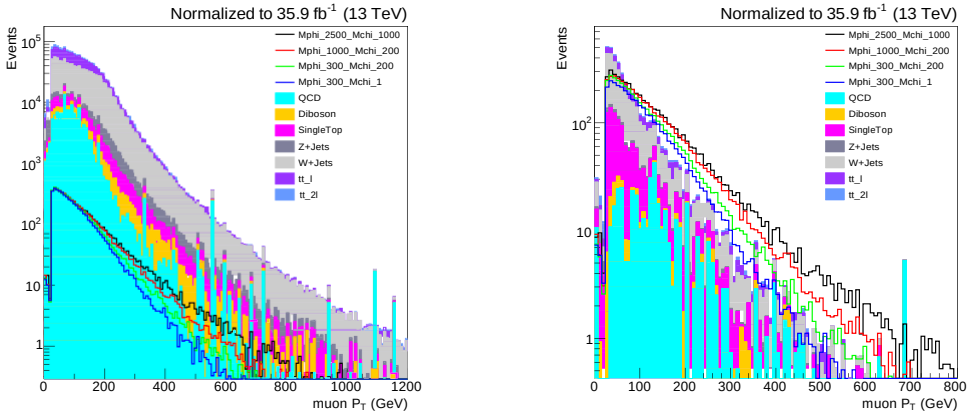

(a) (b)

Figure C-1.: Comparison of (a) muon P_T without cuts and (b) muon P_T with all cuts

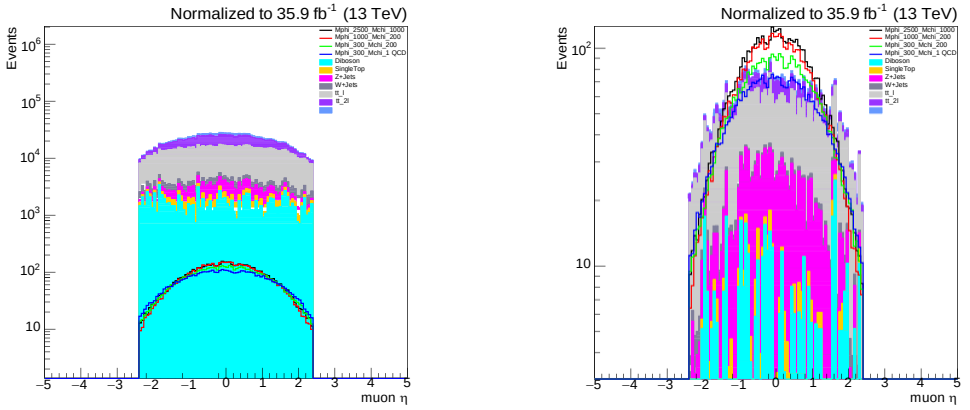

(a) (b)

Figure C-2.: Comparison of (a) muon η without cuts and (b) muon η with all cuts

D. Appendix: Data card

```
imax * number of bins
jmax * number of processes minus 1
kmax * number of nuisance parameters
--------------------------------------------------------------------------------
shapes *          sr        combine.root $PROCESS
--------------------------------------------------------------------------------
bin                       sr      sr      sr      sr      sr
process                   hsig1   tt      ewk     top     qcd
process                   0       1       2       3       4
rate                      -1      -1      -1      -1      -1
--------------------------------------------------------------------------------
```

Bibliografia

[1] Monotop web repository: http://feynrules.irmp.ucl.ac.be/wiki/Monotops.

[2] Tauola Twiki page: https://twiki.cern.ch/twiki/bin/view/CMSPublic/SWGuideTauolaInterface.

[3] Acosta, et a. D.: Measurement of B (tâ↠' W b)/B (tâ↠' W q) at the Collider Detector at Fermilab. In: *Physical review letters* 95.10 (2005)

[4] al, J. B.: "Particle Data Group Collaboration". In: *Phys. Rev D 86, 010001* (2012) [5]

al., Jean-Laurent A.: "Monotop phenomenology at the Large Hadron Collider". In: *Phys.Rev.Lett. 89* (2014)

[6] Alloul, Adam ; Christensen, Neil D. ; Degrande, Celine ; Duhr, Claude ; Fuks, Benjamin: FeynRules 2.0 - A complete toolbox for tree-level phenomenology. (2013)

[7] Alwall, Johan ; Herquet, Michel ; Maltoni, Fabio ; Mattelaer, Olivier ; Stelzer, Tim: MadGraph 5 : Going Beyond. In: *JHEP* 1106 (2011), S. 128. http://dx.doi.org/10.1007/JHEP06(2011)128. – DOI 10.1007/JHEP06(2011)128

[8] Bernabei, R.: Talk at the 10th International Workshop on Neutrino Telescopes. In: *arXiv preprint astro-ph/0305542* (2003)

[9] C., Foundas: "The CMS Level-1 Trigger at LHC and Super-LHC". In: *arXiv preprint arXiv:0810.4133* (2008)

[10] Christensen, Neil D. ; Duhr, Claude: FeynRules - Feynman rules made easy. In: *Comput.Phys.Commun.* 180 (2009), S. 1614–1641. http://dx.doi.org/10.1016/j.cpc.2009.02.018. – DOI 10.1016/j.cpc.2009.02.018

[11] Collaboration, ATLAS: Observation of a new particle in the search for the Standard Model Higgs boson with the ATLAS detector at the LHC. In: *arXiv preprint arXiv:* 1207.7214 (2012)

[12] Collaboration, ATLAS: "Search for invisible particles produced in association with single-top-quarks in proton-proton collisions at $\sqrt{s}$=8 TeV with the ATLAS detector". In: *Eur.Phys. J.C 79* (2015)

[13] Collaboration, CDF: Observation of top quark production in p p collisions with the Collider Detector at Fermilab. In: *Physical review letters* 14 (1995)

[14] Collaboration, CDF: "Measurement of the $t\bar{q}$"production cross section in $p\bar{p}$ collision at $\sqrt{s}$= 1.96 TeV using lepton+jets events with secondary vertex *b*-tagging". In: *Phys. Rev. D 71,* (2008)

[15] Collaboration, CDF: "Search for a dark matter candidate produced in association with a single top quark in *pp* collisions at $\sqrt{s}$=1.96 TeV". In: *Phys.Rev.Lett. 108* (2012)

[16] Collaboration, CMS: "The CMS experiment at the CERN LHC". In: *Journal of instrumentation* (1981)

[17] Collaboration, CMS: "The Electromagnetic Calorimeter Technical Design Report". In: *CERN/LHCC 97-33* (1997)

[18] Collaboration, CMS: "The Hadron Calorimeter Technical Design Report". In: *CERN/LHCC 97-31* (1997)

[19] Collaboration, CMS: "The Magnet Project Technical Design Report". In: *CERN/LHCC 97-10* (1997)

[20] Collaboration, CMS: "The Muon Project Technical Design Report". In: *CERN/LHCC 97-32* (1997)

[21] Collaboration, CMS: "Tracker Technical Design Report". In: *CERN/LHCC 98-6* (1998)

[22] Collaboration, CMS: Addendum to the CMS tracker TDR by the CMS Collaboration". In: *CERN/LHCC 00-16* (2000)

[23] Collaboration, CMS: "The TriDAS project Technical Designal Report, Volume 1: The Trigger Systems". In: *CERN/LHCC 00-38* (2000)

[24] Collaboration, CMS: "The CMS High Level Trigger". In: *The European Physical Journal C-Particles and Fields 46* (2006)

[25] Collaboration, CMS: "Performance study of the CMS Barrel Resistive Plate Chambers with Cosmic Rays". In: *arXiv:0911.4042v2* (2009)

[26] Collaboration, CMS: "Determination of the Jet Energy Scale in CMS with *pp* Collisions at $\sqrt{s}$= 7 TeV". In: *CMS Physics Analysis Summary CMS-PAS-JME-10-010* (2010)

[27] Collaboration, CMS: "Performance of the CMS Cathode Strip Chambers with Cosmic Rays". In: *arXiv:0911.4992v2* (2010)

[28] Collaboration, CMS: Chatrchyan, Serguei, et al. .Observation of a new boson at a mass of 125 GeV with the CMS experiment at the LHC. In: *Physical review letters* 716 (2012)

[29] Collaboration, CMS: ”Description and performance of track and primary-vertex reconstruction with the CMS tracker”. In: *arXiv:1405.6569v2* (2014)

[30] Collaboration, CMS: ”Search for monotop signatures in proton-proton collisions at $\sqrt{s}$=8 TeV”. In: *Phys.Rev.Lett. 1154* (2015)

[31] Collaboration, CMS: ”Search for dark matter in events with energetic hadronically decaying top quark and missing transverse momentum at $\sqrt{s}$ = 13 TeV”. In: *CERN-EP-2017-299* (2018)

[32] Collaboration, TOTEM: ”The TOTEM Experiment at the CERN Large Hadron Collider”. In: *Journal of instrumentation* (2008)

[33] Corcella, G. ; Knowles, I. G. ; Marchesini, G. ; Moretti, S. ; Odagiri, K. ; Richardson, P. ; Seymour, M. H. ; Webber, B. R.: HERWIG 6.5: an event generator for Hadron Emission Reactions With Interfering Gluons (including supersymmetric processes). In: *JHEP* 0101 (2001), S. 010. http://dx.doi.org/10.1088/1126-6708/2001/01/010. – DOI 10.1088/1126–6708/2001/01/010

[34] E. James, M.Mulders Y. M. Y. Maravin ; Neumeister, N.: ”Muon identification in CMS”. In: *CMS Note 2006/010* (2006)

[35] Frixione, Stefano ; Nason, Paolo ; Oleari, Carlo: Matching NLO QCD computations with parton shower simulations: the POWHEG method. In: *JHEP* 11 (2007), S. 070. http://dx.doi.org/10.1088/1126-6708/2007/11/070. – DOI 10.1088/1126–6708/2007/11/070

[36] Higgs, Peter W.: Broken symmetries and the masses of gauge bosons. In: *Physical review letters* 13.12 (1964)

[37] I. Boucheneb, A. D. G. Cacciapaglia C. G. Cacciapaglia ; Fuks, B.: Revisiting monotop production at the LHC”. In: *JHEP 01* (2015)

[38] J. Adrea, F. M. B. Fuks F. B. Fuks: ”Monotops at the LHC”. In: *Phys.Rev.Lett. 84* (2011)

[39] Jindariani, Sergo ; collaboration, CMS: Measurements of top quark properties in top pair production and decay at the LHC using the CMS detector. In: *Nuclear and particle physics proceedings* 273 (2016)

[40] J.M Cela, G. D. ; al., C.Fernández B.: ÇMS Drift Tube Chambers Read-Out Electronics". In: *Conference Report 2008/018* (2006)

[41] Klasen, Pohl M. & Sigl G. M.: Ïndirect and direct search for dark matter". In: *Progress in Particle and Nuclear Physics* (2015)

[42] Klein, Katja: "The CMS Silicon Tracker- Overview and Status". In: *Proceedings of science* (2005)

[43] Lehti, S. ; Karimaki, V.: Computing methods in high energy physics. In: *Lecture Note* (2010)

[44] Malik, et a. Sarah A. A. Sarah A.: Interplay and characterization of dark matter searches at colliders and in direct detection experiments. In: *Physics of the Dark Universe* 9 (2015), S. 51–58

[45] S̈jostrand, Torbjorn ; Mrenna, Stephen ; Skands, Peter Z.: PYTHIA 6.4 Physics and Manual. In: *JHEP* 05 (2006), S. 026. http://dx.doi.org/10.1088/1126-6708/2006/05/026. – DOI 10.1088/1126–6708/2006/05/026

[46] SjÃ¶strand, TorbjÃ¶rn ; Ask, Stefan ; Christiansen, Jesper R. ; Corke, Richard ; Desai, Nishita ; Ilten, Philip ; Mrenna, Stephen ; Prestel, Stefan ; Rasmussen, Christine O. ; Skands, Peter Z.: An Introduction to PYTHIA 8.2. In: *Comput. Phys. Commun.* 191 (2015), S. 159–177. http://dx.doi.org/10.1016/j.cpc.2015.01.024. – DOI 10.1016/j.cpc.2015.01.024

[47] Spataro, Stefano.: Simulation and event reconstruction inside the PandaRoot framework. In: *Journal of Physics: Conference Series* 119.3 (2008)